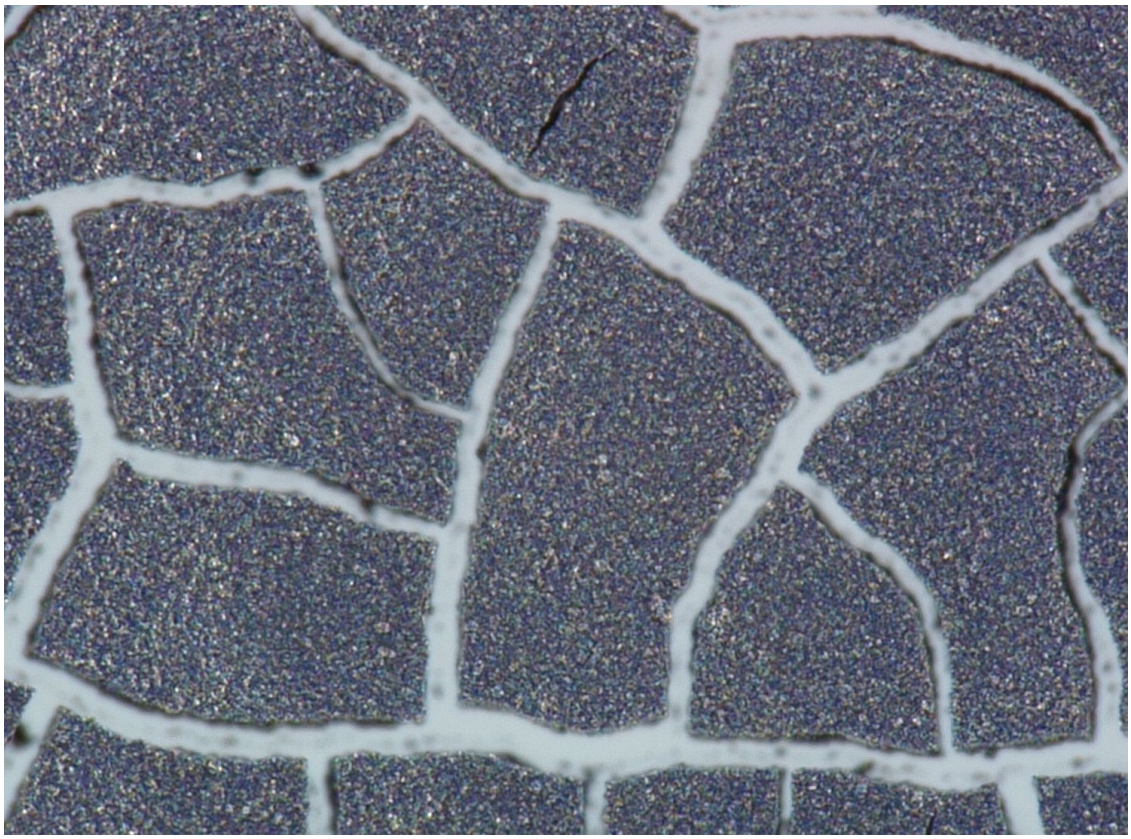

# Investigation of catalyst structure and dispersion methodology on PEMFC catalytic inks and resulting electrodes

Master's thesis in Materials Chemistry

Emma Ulberstad

DEPARTMENT OF PHYSICS
DIVISION OF CHEMICAL PHYSICS
CHALMERS UNIVERSITY OF TECHNOLOGY
Gothenburg, Sweden 2023
www.chalmers.se

Master's thesis 2023

# Investigation of catalyst structure and dispersion methodology on PEMFC catalytic inks and resulting electrodes

EMMA ULBERSTAD


CHALMERS
UNIVERSITY OF TECHNOLOGY

Department of Physics
*Division of Chemical physics*
Chalmers University of Technology
Gothenburg, Sweden 2023

Investigation of catalyst structure and dispersion methodology on PEMFC catalytic inks and resulting electrodes
EMMA ULBERSTAD



Supervisor: Felix Ernst, Powercell group
Examiner: Björn Wickman, Department of Physics

Master's Thesis 2023
Department of Physics
Division of Chemical physics
Chalmers University of Technology
SE-412 96 Gothenburg
Telephone +46 31 772 1000

Typeset in LaTeX
Printed by Chalmers Reproservice
Gothenburg, Sweden 2023

Investigation of catalyst structure and dispersion methodology on PEMFC catalytic inks and resulting electrodes

EMMA ULBERSTAD
Department of Physics
Division of Chemical Physics
Chalmers University of Technology

# Abstract

The demand for green energy increases every year, pushing the development of sustainable energy sources. Proton exchange membrane fuel cells (PEMFCs) are a promising technology for renewable energy conversion due to their clean emissions and high energy-conversion efficiency. The electrodes are a core part of PEMFCs, containing the catalyst at which the electrochemical reactions occur, where hydrogen and oxygen are converted to water and energy. To enhance cost efficiency, performance and durability of PEMFCs, it is essential to better understand the complex and partly unknown properties of the electrode and optimize the electrode production process. There is a need to better understand the dispersion method of the catalyst ink that makes up the electrode because it is one of the major factors determining the electrode properties. The effect of catalyst ink materials, dispersion technique and parameters on the catalyst ink microstructure were studied using rheological measurements and light microscope imaging of the electrodes. Dispersion by ultrasonication at higher vibrational amplitude showed an increase in viscosity and less visible agglomerates on the electrode surface as compared to lower amplitudes. A continuous decrease in apparent agglomerate size and abundance was found with increasing ultrasonic energy input. The results also showed a partly unexpected rheological trend where highly dispersed inks exhibit poorer rheological properties, such as low viscosity and elastic modulus for the applied coating method as compared to less dispersed inks. Ultrasonication and bead-milling dispersion method resulted in inks with different rheological properties. The investigation showed that rheology and microscopy are able to only partly capture the complex characteristics of the agglomerated structures and complimenting techniques like e.g. SEM and DLS can help further investigation. With this work, an optimization of the ink dispersion process was achieved and further insight into the dispersion parameters allowed to establish dispersion design rules, e.g. regarding the ultrasonic power and energy input, and to further elucidate the interdependency between ink components and dispersion methodology.

Keywords: proton exchange membrane fuel cell, catalyst, rheology, catalyst layer.

# Acknowledgements

I would like to begin by thanking Powercell for the opportunity to do my Masters thesis together with them. Then I would like to thank my supervisor Felix Ernst for his support, helpful input and for providing the theoretical background necessary to conduct this thesis. I would also like to thank all my family for the support and a special thanks to my friends at "studiecentrum" for providing me a safe place to come and seek support and encouragement during hard times. Without you this thesis would never have been completed.

Emma Ulberstad, Gothenburg, May 2023

# List of Acronyms

Below is the list of acronyms that have been used throughout this thesis listed in alphabetical order:

| | |
|---|---|
| BL | Backing layer |
| CB | Carbon black |
| CCL | Catalyst coated layer |
| CCM | Catalyst coated membrane |
| CL | Catalyst layer |
| ECSA | Electrochemical surface area |
| FC | Fuel cell |
| GDE | Gas diffusion electrode |
| GDL | Gas diffusion layer |
| GC | Graphetized carbon |
| HOR | Hydrogen oxidation reaction |
| HSC | High surface area carbon |
| I/C | Ionomer/carbon |
| LSC | Long side chain |
| MEA | Membrane electrode assembly |
| MPL | Microporous layer |
| NP | Nanoparticle |
| ORR | Oxygen reduction reaction |
| PEM | Proton exchange membrane |
| PEMFC | Proton exchange membrane fuel cell |
| PFSA | Perfluorocarbonsulfonic acid |
| Pt | Platinum |
| SSC | Short side chain |
| wt.% | Weight percent |

# Contents

# List of Figures

# 1

# Introduction

## 1.1 Background

The increasing global demand on energy from the human population in combination with the efforts to reduce $CO_2$ emissions have pushed the research and development of renewable energy sources. One of the most promising energy technologies for renewable and sustainable energy conversion is the fuel cell. Fuel cells (FCs) have the potential to replace fossil fuels in mobile applications, as well as in stationary and portable power sources (1). FCs stand out from other energy conversion technologies because of their lack of pollutants, high energy-conversion efficiency and low operating temperatures (2). It is very likely that FCs will be an important part of the modern energy technology in the future (3).

The principles behind the fuel cell was first demonstrated in the year of 1839 by the scientist Sir William Grove that a few years later also developed the first fuel cell (4). However, it would take all the way until 1952 for the first practical 5 kW fuel cell stack to be constructed, then by Franic T. Bacon. Since the 50s tremendous progress has been made and several types of fuel cells have been developed. Due to numerous advantages such as viability, efficiency and quick start up time, the proton exchange membrane (PEM) is the most commonly used fuel cell type today.

PEMFCs produce electricity through electrochemical reactions of $H_2$ and $O_2$ to produce water, meaning that no other products like $CO_2$ or pollutants are being emitted (4). Despite the advantages with FCs and recent progress, there are still improvements that has to be made in order to meet the needs of the market and reach commercialisation success. In order to enhance the performance and improve the durability, all components in the fuels cell has to be taken into account.

The greatest limitation with PEM fuel cells today are their durability and cost. Even though fuel cells already have been demonstrated in many applications, the cost has to be reduced to make them more available for normal commodities. The biggest limiting factor is the use of expensive platinum group metal catalysts that can contribute to up to 55% of the total cost of a fuel cell system (5). The platinum group metal catalysts are critical for the electrochemical reactions taking place in the fuel cell and a lot of research is focused on reducing the use of catalyst without reducing the performance.

To achieve a lower loading of catalyst without decreasing performance, a high utilization of the catalyst is essential (6). The utilization of a catalyst is defined as the ratio of the electrochemical active surface area (ECSA), which is the area accessible for electrons and protons to react at, to the total surface area of the catalyst. To increase the ECSA, catalyst particles in the nanometer range are used that are supported on slightly larger carbon particles for stabilization. Due to the high surface energy of the carbon support, they tend to gather and form prominent clusters to lower the energy which results in an decrease in electrochemical active surface area compered to well separated particles. To break up these clusters and increase the catalyst utilization, different dispersing methods are commonly used. However, it is not well understood how different dispersion parameters effect the structure of the catalyst layer and finally the performance of the electrode in the fuel cell.

## 1.2 Objective

There are numerous studies describing the preparation of catalytic inks for PEM fuel cell, but due to complex interactions, there is a lack of knowledge on how preparation method effects the final electrode. This thesis investigates the influence of catalyst characteristics together with dispersion methodology to better understand the influence it has on the catalyst inks and the resulting electrodes. Characteristics of the catalytic inks that is being investigated is support structure, Pt loading on support, ionomer type and the catalyst preparation method. Both high surface area carbon and graphitized carbon supported catalysts are investigated, as well as pure carbon support. The catalyst inks are dispersed using different dispersion techniques, e.g. ultrasonication and bead-milling. The goal is to understand how the power, energy and sonication setup affects the ink for ultrasonication, how different types of catalyst get affected and finally how these parameters affect the electrochemical surface area and the sub-scale MEA performance. The measurements for the catalysts will also be compared to those of pure carbon support to understand the effects the Pt has in the stability of the ink.

This thesis first present the necessary theoretical background on fuel cells and the catalyst in chapter 2. Then the applied methods will be presented in chapter 3 and followed by the results and discussion presented in chapter 4. Lastly are the conclusions presented in chapter 5.

# 2

# Theory

This chapter provides a relevant theoretical background on the concepts discussed in this thesis. The theory behind the proton exchange membrane fuel cell and the components of the membrane electrode assembly is presented as well and the theory behind the methods used for analysis.

## 2.1 The Proton Exchange Membrane Fuel Cell

A range of different FC types exists today, but the one type that has drawn the most attention in mobile applications is the Proton exchange membrane fuel cell (PEMFC). This is due to the PEMFCs simplicity, viability and quick start up, which also has led the PEMFC to be demonstrated in many different applications, ranging from automobiles to airplanes (4). The general principles of the PEMFC is the same as for all types of FCs, it continuously and directly converts chemical energy from fuel and oxidant to electrical energy in the form of a DC current.

The unique component of the PEMFCs is the proton exchange membrane (PEM), this membrane is placed in between two electrodes forming the so called membrane electrode assembly (MEA) (7). The PEM has a high proton conductivity and very low penetrability to gases, creating a barrier between the fuel and reactant gases while still letting protons pass through. The electrodes consists mainly of carbon, ionomer and catalyst, and it is on the catalyst surface at the electrode and membrane interface the electrochemical reaction takes place. Hydrogen gas is supplied to one of the electrodes, the anode, where it is split into protons and electrons in the so called hydrogen oxidation reaction (HOR).

$$\mathrm{H_2} \longrightarrow 2\,\mathrm{H^+} + 2\,\mathrm{e^-} \tag{2.1}$$

The protons pass through the PEM to the cathode while the electrons go through the electrically conducting electrode, through current collectors and then though a external circuit, creating an electrical current. At the cathode, oxygen is fed and on the catalyst surface at the electrode and membrane interface the oxygen reduction reaction (ORR) occurs where electrons, protons and oxygen is reacting to form water.

$$\frac{1}{2}\,\mathrm{O_2} + 2\,\mathrm{H^+} + 2\,\mathrm{e^-} \longrightarrow \mathrm{H_2O} \tag{2.2}$$

By combining reaction 2.1 and 2.2 the net reaction of the FC becomes

$$\mathrm{H_2} + \frac{1}{2}\,\mathrm{O_2} \longrightarrow \mathrm{H_2O} \tag{2.3}$$

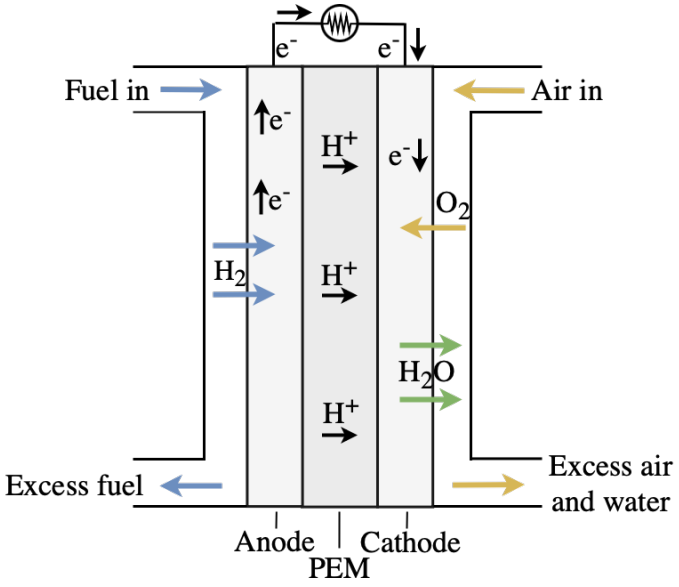


**Figure 2.1:** Schematic figure of the PEMFC and the flow of reactants and products.

This means that the only byproduct emitted from the FC is pure water. The electrochemical reactions and the flow of reactants and products are shown in Figure 2.1. The ORR is kinetically much slower compared to the HOR (7). The hydrogen molecules are relatively easy spilt in the present of a platinum catalyst, but it becomes more difficult to split the more strongly bound oxygen molecules. This limits the electrochemical reaction and the FC performance. The catalyst loading can be increased to further accelerate the reaction but that solution is limited by scaling and economic problems (2). Because of this, several studies have focus on the development and optimizations of catalyst material and electrode structure to achieve high-preforming cathodes with high catalyst utilization.

### 2.1.1 The Oxygen Reduction Reaction

The oxygen reduction reaction is the kinetically limiting step of the electrochemical reaction, hence limiting the fuel cell performance. Because of the relatively sluggish kinetics, a lot of research has been made in order to try to understand the mechanism behind the reaction (8). The mechanism of the ORR is relatively complicated with several intermediate steps that is dependent on the electrode material, catalyst and electrolyte. The maximum amount of electrical energy generated by a fuel cell is corresponding to Gibbs free energy, meaning that the theoretical maximum voltage of a single cell can be calculated by dividing Gibbs free energy by Faraday´s constant and the number of electrons of $H_2$. This calculation results in the theoretical maximum to be 1.23 V. The actual operating value voltage however is lower due to various losses to which the slow kinetics of the ORR have a sgnificant contribution (9).

The losses are called polarization when the cell voltage is compared to the experi-

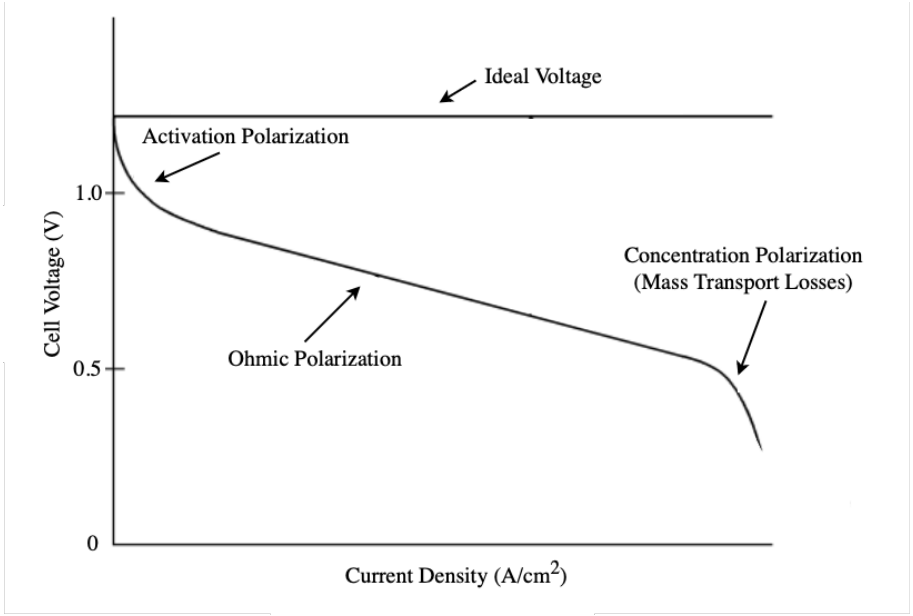


**Figure 2.2:** Graph of the cell voltage against current density for the ideal fuel cell and a actual one.

mental equilibrium cell voltage (10). The greatest losses are the overpotential and overvoltage that are mainly a result from the activation polarization, ohmic polarization and concentration polarization (11). The activation polarization loss is dominant at lower current densities. The ohmic polarization increase with increasing current and the concentration polarization only becomes prominent at high limiting currents. The cell voltage versus the current density is showed for the ideal case and a actual case in Figure 2.2.

The activation polarization is associated with sluggish reaction kinetics and low catalyst activity (10). This means that the activation polarization is directly related to the reaction rate of the electrochemical reactions. The electrochemical reaction involves an activation energy that needs to be overcome by the reactants and the voltage drop due to this activation polarization is often described by the Tafel equation, showed in Equation 2.4.

$$\eta_{act} = \frac{\mathrm{RT}}{\alpha \mathrm{nF}} \ln \frac{i}{i_0} \tag{2.4}$$

where R is the gas constant, T is the temperature, $\alpha$ is the electron transfer coefficient, F is Faraday´s constant and $i_0$ is the exchange current density. Tafel plots are used to measure the exchange current density and gives a visual presentation of the activation polarization of the FC.

### 2.1.2 Proton Exchange Membrane

The PEM is at the heart of the PEMFC. Its main function is to facilitate the transportation of protons from the anode to the cathode. The membrane must have good

proton conductivity, low permeability for gases to keep the fuel and oxygen separated, and be chemically and mechanically stable in the fuel cell environment (12). Different types of membranes have been tested in the PEMFC, but the material most often used for the membranes today is perfluorocarbonsulfonic acid (PFSA) ionomer, commonly Nafion by Dupont due to its suitable properties. The $SO_3H$ group on the PFSA is ionically bonded, meaning that on the end of the side chain is actually an $SO_3^-$ ion with an $H^+$ ion, hence the name ionomer (12). The backbone of the ionomer is highly hydrophobic but because of the ionically bonded $H^+$, the side chains become highly hydrophilic. This makes it possible for the ionomer to adsorb relatively high amounts of water. The adsorbed water is what enables the movement of protons, making the membrane proton conducting.

The proton conductivity is highly dependent on the water content and overall membrane structure. The conductivity increases with water content up to a certain level where continued water adsorption decrease the proton concentration and the conductivity is decreased (7). The thickness of the membrane strongly influence its properties and lifetime. Thinner membranes have higher proton conductivity and increased performance efficiency but have lower physical strength and higher gas permeability that ages the membrane faster. A relatively thin membrane with chemical and mechanical stability is desired.

### 2.1.3 Electrode Structure and Components

The electrode is constructed with a catalyst layer (CL) and a gas diffusion layer (GDL) (1). The GDL does in turn consist of two layers, a microporous layer (MPL) consisting of carbon powder and usually an ionomer and a backing layer (BL) of carbon paper or carbon cloth. A simple structure of the electrode structure is showed in Figure 2.3. The electrochemical reaction occurs on the electrode, therefore it needs to have good electronic conduction to allow the produced electrons to flow from the anode to the cathode. The electrode also needs to have pores of suitable sizes for the transport of reactant gases through the electrode. To achieve these properties, the electrode usually consists of catalyst particles on a electrically conducting carbon particle support and an ionomer for proton conduction.

#### 2.1.3.1 The Catalyst Layer

The CL is a critical component of the PEMFC with several design variables that needs to be optimized. There are several properties that the CL needs in order to meet the desired FC performance (13). A high performing CL has good electrical and proton conductivity, efficient transport of reactant gases and water and high catalyst activity and catalyst utilization. The CL usually consists of catalyst, carbon powder and ionomer (1). The purpose of the ionomers is to facilitate proton transport from the anode to the cathode. Carbon powder is used both for its good electrical conductivity and also as a support for the catalyst to increase utilization. PTFE is often used to bind to the catalyst and increase the hydrophobicity.

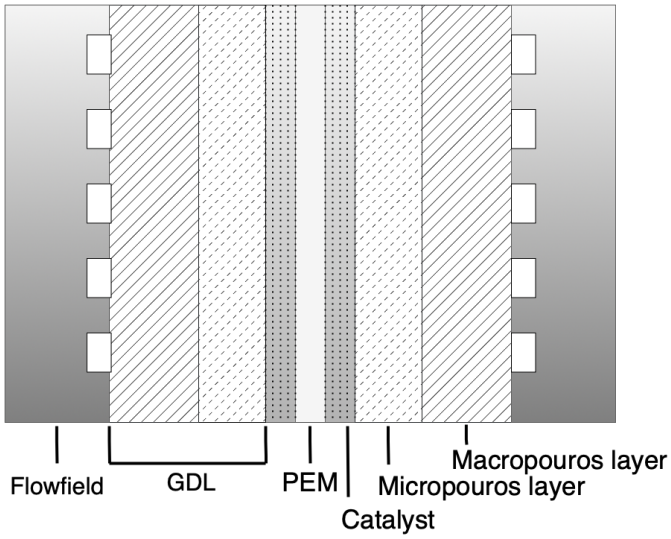


**Figure 2.3:** Figure showing the different parts of of the electrode, including the PEM in the centre, the catalyst layer, GDL and flow field.

It is essential that the CL have good electronic conductivity to allow for the produced electrons to flow through, as well as good protonic conductivity to allow the flow of protons from the anode to the membrane. The CL should be optimized based on the desired level of adsorption of reactants, hydrophobicity and ionic and electrical conductivity. The electrochemical reaction can only take place at the boundary between catalyst, ionomer and void, the so called three-phase boundary, shown in Figure 2.4. This is because it is the only place where all the reactants have access. The electrons can only travel through the electrically conducting compounds, the protons can only go trough the ionomer, and the gases can only travel trough the pores.

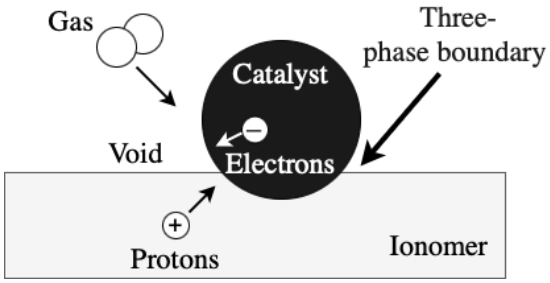


**Figure 2.4:** Schematic representation of the boundary between catalyst, ionomer, and void where the electrochemical reactions occurs.

The ionomer used for proton conduction in the CL is often Nafion, facilitating the flow of protons trough the anode to the PEM and lastly the cathode (1). The ionomer and its hydrophilic group allows for the adsorption of water and hence the ionic conductivity as well as binding to the catalyst giving it more electrochemical surface area. The concentration of ionomer is critical as a too low concentration gives a poor ion conductivity and a too high concentration results in poor gas diffusion.

The method used when fabricating the MEA strongly influence the resulting CL microstructure. The fabrication process usually involves three steps staring with the mixing and dispersion of the components making up the catalyst ink (14). The ink is then coated onto a membrane/film or straight on the GDL forming a catalyst coated membrane (CCM) or gas diffusion electrode (GDE). Finally, after the ink has dried, is the CCM or GDE hot-pressed or assembled to form the MEA.

There are three methods that are commonly used for fabricating MEAs. The first involves adding a mixture of carbon supported catalyst, PTFE, ionomer and sometimes solvent straight to the GDL using an appropriate technique (15). The coated GDL is then hot-pressed onto a membrane that has been pre-treated with catalyst on each side. For the second method, a mixture of catalyst and PTFE is directly added to the membrane using different methods. The GDL is then applied when the catalyst has been fixed to the membrane. The third method is similar to the two previously mentioned methods and is used in this thesis. The CLs are made via the mixing of an ink consisting of the Pt catalyst on a carbon support structure and an ionomer that are dispersed in a water-alcohol solvent matrix. The ink is then coated onto a substrate and dried, forming the CL. The CL microstructure is controlled by the interactions between Pt, carbon support, ionomer and solvent as well as production processes like coating and drying. But these interactions and what impact they have on the ink is not very well understood. More insight is also needed on the effects that of processing method and conditions have on the final electrode.

As of right now, there is a lack of knowledge on how to design the CL with an optimum microstructure for better fuel cell performances. It is critical to better understand the influence of different components and processing methods have on the CL and the final electrode to reduce cost and increase performance of PEMFCs. The choice of catalyst heavily impacts the characteristics of the catalyst ink, such as the microstructure, Pt loading and Pt particle size. Investigating these characteristics together with dispersion methodology will lead to a better understanding of the influence it has on the inks and resulting electrodes.

#### 2.1.3.2 The Gas Diffusion Layer

The performance of the PEMFC is strongly influenced by the properties of the GDL. The GDL is made of carbon and PTFE with the main purpose to facilitate gas diffusion, guiding water to prevent flooding and allow conductivity. The GDL is also important for the interaction with the bipolar plates as it connects the CL to the bipolar plates and acts as a current collector. The mechanical properties of the GDL, such as thickness, compressibility and elastic modulus, also influence the overall stack mechanistics. The MPL on the CL side increases the catalytic activity because it decreases the saturation of water (1). The type of carbon substrate used in the MPL or CL is one of the most important parameters controlling the GDL properties. The MPL is made of a mixture of carbon powder and PTFE and is the part that contributes the most to the porosity for gas flow. The MPL must

have high electrical conductivity, be a good catalyst support with high surface area and be corrosion resistant. The properties of the carbon powder strongly influence the performance and durability of the PEM fuel cell. The BL is mostly used as a supporting layer for the electrodes, but also helps keeping moisture away from the electrodes and helping diffuse gas and provide routes outside of the electrode for electrons and water. The BL commonly consists of carbon, as it needs to be acid resistant, have good gas permeability and electrical conductivity, being elastic under compression and lastly being able to maintain porosity.

## 2.2 Catalyst

The catalyst plays an particularly important role in maximizing the FC performance. As stated in Chapter 2.1.1 is the catalyst composition and structure one major factor influencing the overpotential of FC reactions. The catalysts used in PEMFC can be divided into three groups. These are platinum based catalysts, platinum modified based catalyst and non-platinum based catalyst (16). Although effort has been put into finding less expensive non-Pt-based catalysts, no other alternative have as low overpotential and high catalyst activity and durability as the Pt based catalysts. Pt-based catalysts are also less sensitive to the harsh acidic environment that is present in PEMFCs. Hence is the Pt-based catalysts the best know catalyst for the fuel cell reactions (14), but it is limiting the widespread commercialisation of PEMFCs due to high cost and scarcity (17). According to Guo et. al. (5), Pt could make up as much as 55% of the total manufacturing cost of PEMFCs. To reduce the cost, development is directed to use the Pt more efficiently and hence reduce the amount needed. When PEMFCs first was developed, pure Pt nanoparticles (NPs) were used as catalyst which required the loading to be as high as 28 mg/cm$^2$. In the late 1990s the carbon supported catalyst structure was introduced and the required loading dropped to 0.3-0.4 mg/cm$^2$ (1). The high surface area carbon support structure allows for the Pt particles to be distributed uniformly on the surface, resulting in a maintained high ECSA of the Pt particles (18).

Different types of support structure can be used, such as carbon nanotubes, carbon nanofibers, graphenes and carbon black. In addition to allowing for highly dispersed Pt NPs, the support structure also influence the durability of the catalyst and can interact with the Pt and influencing the catalytic activity (19). Much effort has been put into developing novel catalyst support structures for enhanced durability and catalytic activity but one of the most common support material today is the Vulcan XC-72 carbon black support. There are also various of alloys of Pt and metals like Co, Ni and Fe that show highly increased catalytic activity despite decreased Pt loading(18). However, the Pt alloy catalyst show poor durability because the harsh fuel cell environment results in dissolution and oxidation of the alloy metals. Efforts are being made to further develop the Pt alloy catalysts but the pure Pt catalyst remains the most popular catalyst for the PEMFCs.

Despite being the best alternative, Pt NP catalysts are still subject to dissolution, coalescence and poisoning that decrease the catalyst surface area and increase the

overpotential of the fuel cell reactions (5). The catalytic ink used in the thesis to make electrodes for PEMFC consists of pure Pt NPs on carbon black support, ionomer and solvent. Even though all these components play a crucial role for the final electrode, little is known about the influence they have (1). For the catalyst layer the goal is to have the highest reactivity with the lowest amount of catalyst. This requires a large amount of electrochemically active surface area as well as small kinetic barriers for bulk transport and interfacial transfer electrons, protons and reactants. Most research have been focused on Pt based catalyst and the effect of Pt content and particle size on the performance. Besides this, much research has also gone into the carbon structure of the CL, the manufacturing method, influence of solvent matrix and hydrophobic substances, surface structure, porosity and the degradation of Pt. The CL microstructure controls the transport properties of electrons, protons, reactants and products and hence controls the whole fuel cell performance.

### 2.2.1 Catalyst Design

Two of the greatest improvements made to the catalyst layer design have been the incorporation of Pt NPs as well as the impregnation or colloidal mixing of the high surface area carbon support with ionomer. NPs have a drastically greater surface area compared to the corresponding bulk material, so the use of Pt NPs in the catalyst layer enabled for a drastic reduction of the catalyst loading without decreasing the total ECSA. The use of impregnation or colloidal mixing of the high surface area carbon support with the ionomer makes sure that protons can reach the Pt surface throughout the whole CL. These preparation techniques have been improved over time and is today the standard method for CL fabrication.

The mass activity of a catalyst is defined as the current normalized by the catalyst loading measured at a specific potential times the specific ECSA (14). The mass activity can be improved by increasing the specific ECSA by decreasing the particle size, meaning that the Pt loading can be decreased by decreasing the Pt particle size. The properties of NPs are very sensitive to particle size and several studies have found that the mass activity is not inversely proportional to particle size, and decreasing the particle size to much can result in less desirable properties. According to Antolini et. al. (14) goes the dependence of mass activity of Pt on particle size through a maximum where the optimal particle size is around 3 nm for the ORR. The particle-support interactions may also change the specific activity as the smaller Pt particle have more surface atoms interacting with the carbon support compared to larger particle. These interactions improve the charge transfer between the Pt particle and carbon support which can change the catalytic activity. Studies have found that the electrochemical surface area of the electrodes decreases over time when running a PEMFC, resulting in degradation of the performance of the fuel cell (20; 21). The performance decay rate of the electrodes are strongly correlated to the Pt particle size (22). Potential cycling in the typical operation voltage range for mobile FC applications accelerates Pt dissolution and carbon corrosion which change the catalyst activity and lead to irreversible performance loss. The dominant degra-

dation process that occurs during these conditions are Pt aggregation-coalescence on the carbon support surface, Pt dissolution-deposition and Ostwald ripening, but Pt detachment via carbon corrosion also occurs. Smaller particles are more sensitive to these degradation processes and hence show greater decay rates as compared to larger particles. The Pt particle size range that show both optimized performance and durability has been found to be between 4–6 nm.

### 2.2.2 Catalyst Agglomeration

The interactions between the Pt NPs, the CB support and the ionomer are complex which is reflected in the formation of the CL. The self-organization of ionomer and Pt/CB particles in colloidal ink solutions results in phase separation and agglomeration (23). The Pt/CB primary particles has a tendency to form larger aggregates that in turn cluster to form predominant entities known as agglomerates. With these large agglomerates of Pt/CB, a lot of catalyst is not utilized.

How well the ionomer can penetrate and break up these agglomerates are depending on the fabrication technique, ionomer concentration, type of carbon support and formation kinetics of the agglomeration (23). For most cases can the ionomer not break up the agglomerates and just attaches itself to the surface instead. The agglomerated structure usually have a bimodal pore size distribution where Pt/CB particles form primary pores of less then 2 nm and secondary pores are formed between agglomerates of over 50 nm. Hence, the CL structure contains particles and pore of a wide range of length scales, which implies a hierarchical structural picture for the CL (13). Many studies have shown that the microstructure and composition of the agglomerates strongly influence the performance of the CL and it is important to understand whether the ionomer can penetrate into the primary pores of the agglomerates to form a proton conducting phase or if it can only be formed in the secondary pores between agglomerates. By mixing the ionomer with the dispersed Pt/CB in the ink before deposing it to form a CL, the interfacial area between Pt and ionomer is increased which increase the catalyst utilization.

Ionomers like Nafion is often used as binder in PEM fuel cells. The concentration of ionomer in the CL influences the gas permeability, catalytic activity and ionic conductivity and should therefore be optimized to reduce the resistance and hence increase the utilization of the catalyst (24). In modern fuel cells, the ionomer is used both as binder in the CL and in the PEM to extend the three-phase interface where the electrochemical reaction occurs, and hence increases the catalyst utilization.

## 2.3 Dispersion

Processing of the catalyst ink is necessary to break up agglomerates, achieve smaller particle sizes and utilize the catalyst more (25). The effect of dipsersion on the CL microstructure is illustrated in figure 2.5. The most commonly used processing

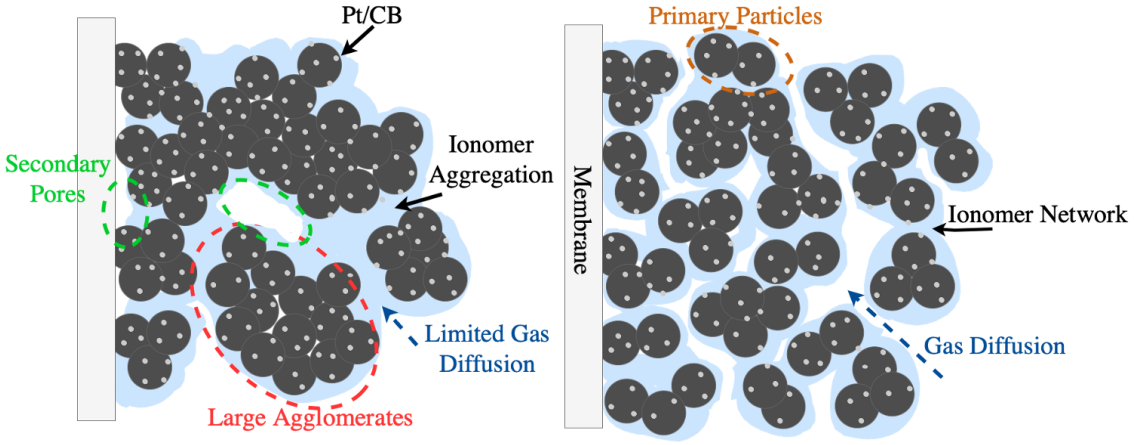


**Figure 2.5:** Schematic figure showing the difference in microstructure for poorly dispersed (left) and well dispersed (right) CL.

methods, or dispersion methods, are ball-milling and ultrasonic dispersion. Both methods yield very different results depending on how the treatment is performed and several studies have tried to find an optimized treatment to improve catalyst activity (26).

### 2.3.1 Ultrasonic Dispersion

Ultrasonic dispersion is used to break up the agglomerates that form in the ink solution. When the ink solution is exposed to ultrasound, the sound waves creates high- and low-pressure cycles through the liquid (27). During the low-pressure cycle the high-pressure waves creates small vacuum bubbles. These bubbles increase in size until they reach a point where they no longer can adsorb more energy and then violently collapse, which is called cavitation. Cavitation is a secondary effect but is the main reason for the observed effects of ultrasound. The implosion of the cavitation bubbles causes extreme forces where the large negative pressures are strong enough to overcome intermolecular forces binding the liquid. When the cavitation bubble collapse, hot-spots in the fluid are created with temperatures up to 5000 K, pressures up to 20 MPa and jets of liquid with velocities up to 280 m/s (28; 29). These jets push liquid with high pressure in between the particles in the agglomerates and force them to separate. The jets also accelerates small particles to high velocities causing collisions at high speed that break up agglomerates. The cavitation bubbles have a lifespans of less than 0.1 $\mu$s and are cooled in rates above $10^{9-10}$ $Ks^{-1}$.

The two most common methods for ultrasonication is either to use an ultrasonic bath or an ultrasonic probe. The ultrasonic bath usually consists of a stainless steel tank with piezoelectric transducers attached underneath (29). The sample vial is places in the tank that transfer the ultrasonic waves to the sample. While the ultrasonic bath has advantages such as good energy distribution through the sample vial, relatively good temperature control, no need for special vessels and being inexpensive, they have disadvantages like poor transmission of power into the sample vessel and fixed ultrasonic frequency and power input that cannot be changed. To

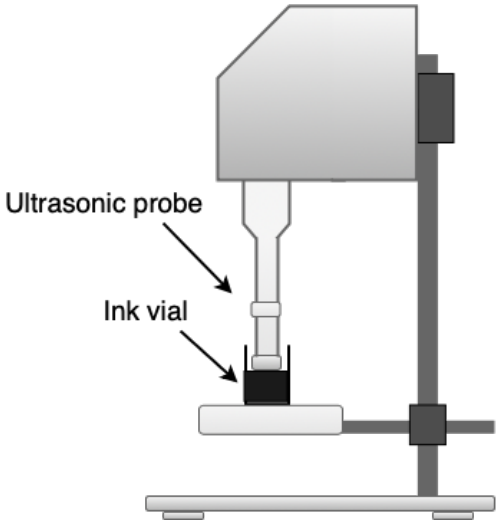


**Figure 2.6:** A schematic illustration of the ultrasonication setup with a sample vial placed under the ultrasonic probe.

overcome the disadvantages of the ultrasonic bath is the ultrasonic probe designed to be placed directly into the sample. This way can the probe transfer the power directly to the sample and does not need to rely on the transfer through the water or vessel walls, allowing for higher amounts of ultrasonic power. The ultrasonic probe setup consists of a specially designed metal rod that is connected to the transducers. A schematic image of the setup is shown is Fig. 2.6 where the ink vial has been placed under the ultrasonic probe that is connected to a stand. The ultrasound is transferred to the sample via the probe tip and the ultrasonic intensity and vibrational amplitude of the probe can be altered by changing the power input and the power put into the system can be changed by varying the shape and size of the probe.

In this work an ultrasonic probe is used as it allows for changes in ultrasonication energy, can reach higher energies and be used with different accessories then the ultrasonic bath. It has been found that ultrasonic treatment of catalyst ink with an ultrasonic probe have a significant effect on increasing the ECSA and that changing parameters such as frequency, power, time etc, yield different results (30). It has also been found that dispersing the ink for longer amounts of time can be damaging to the composition and resulting in a decrease in ECSA. Previous work have also showed that cooling during sonication treatment is important to avoid heating and sintering of the Pt NPs (31). To be able to optimize the dispersion process, it is important to understand how different inks behave during dispersion and what effect different catalysts, solvent matrix and ionomers have on the break down of agglomerates. An insufficient amount of sonication will result in poor dispersion of the agglomerates, while excessive sonication can damage the Pt/CB structure which also leads to a decrease in ECSA (25).

### 2.3.2 Bead Milling

Bead milling is another dispersion process that is commonly used. The process is very different from ultrasonication which result in different rheological and thixotropical properties (26). The principle behind bead milling is very simple, zirconium balls of desired size and amount is added to the catalyst ink bottle which is then placed on a machine that rolls the bottle on its side. When the bottle rolls, the beads inside that are covered in catalyst ink will roll around each other and grind down the agglomerates, illustrated in Fig. 2.7. As the beads bump into and chafing against each other, the ink in between the beads are getting dispersed. The machine used in this work to roll the ink bottles is called a roller-shaker. The machine both roll the bottles on their side at an adjustable speed as well as tilting the bottles back and forth horizontally.

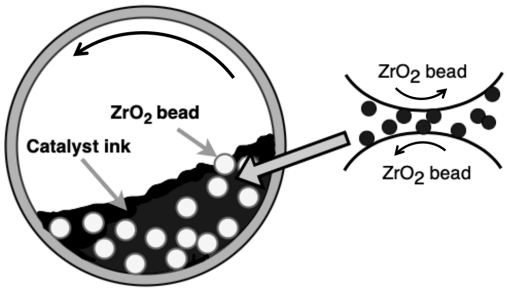


**Figure 2.7:** A schematic figure of the ink vial during bead milling. A closed-up image show of how the ink particles are grinded against the $ZrO_2$ beads.

## 2.4 Electrode Fabrication

The fabrication process of the electrode influence the resulting electrode structure and hence the fuel cell performance and degradation (32). The currently most used methods for electrode fabrication are air-spray coating, ultrasonic spray and slot-die coating. The air spray coating technique is being replaced by the ultrasonic spray technique because it produces more uniform coatings but the cost is also much higher for the ultrasonic spray system compared to the air-spray. The slot-die technique is widely utilized in several industries for large scale manufacturing of high area films with roll-to-roll compatibility. The benefits of slot-die coating the thickness control, non-contact coating mechanism, scalability and the potential of lower the cost by improved production rate. The roll-to-toll compatibility is a benefit because that manufacturing process can increase the fabrication speed of CL by over 500 times compared to lab-scale spray coating (33). With the slot-die technique is the ink solution directly coated onto the substrate via the coating head while the substrate moves underneath (34). The wet thickness is determined by the amount if ink that is placed on the substrate.

### 2.4.1 Doctor Blade

A widely used, scalable and similar technique to the slot-die technique is the doctor blade coating. The doctor blade coating technique was used in the experimental part of this thesis. For this technique a blade is running over the substrate with a small gap that determines how much ink can get trough, effectively spreading the ink over the substrate (34). The advantages of this method is that it can be scaled to industrial manufacturing, it is quick, efficient and simple, and creates uniform thin films over large surfaces with low ink wastage. When the ink is being coated, it is subject to different shear environments. It is hence important to have an ink with desired rheological properties to achieve high-quality, continuous and defect-free coatings. Different coating methods require different rheological properties, for the doctor blade an relatively viscous ink is desired but a too viscous ink will result in poor flowability with poor distribution and weak adhesion to the substrate. The catalyst ink is a multi-phase fluid system that in most cases exhibit shear-thinning behavior (33). The shear-thinning behavior originates from for example the break up of large agglomerates to smaller ones by shear force, the initially tangled ionomer chains disentangle by the shear force and disordered particle aligning with the flow. Alcohol and water that are commonly used as solvents in catalyst inks are Newtonian fluids and when dispersing ionomer into the solvent the dispersion solution still approaches Newtonian behavior for shear forces above 10 $s^{-1}$. When dispersing Pt/CB in the solvent, is shows a shear thinning behavior and for almost all cases do a solution with Pt/CB, ionomer and solvent show a shear thinning nature. When a shear force is applied to the ink, the primary and secondary agglomerates will align with the flow, and the secondary agglomerates might break down to smaller secondary agglomerates or primary agglomerates, resulting in a shear thinning behavior. During the coating process will a shear-thinning ink be subject to deformation, showing a different microstructure compared to the ink. The shear-thinning behavior complicates the relations between the catalyst ink microstructure and the CL structure but also contributes to the uniformity and thickness control of the CL during coating.

### 2.4.2 Decal Substrates

The decal transfer method was used in this thesis, which means that the CL is first coated onto an inert decal substrate that is then transferred to the membrane via hot pressing, producing the CCM. The type of decal used influence both the coatability and tranferability of the CL (33). There are different reinforces and non-reinforced decals of different materials, with polytetrafluoroethylene (PTFE) being one of the most commonly used materials. In addition to being inert, the decal should not poison the catalyst during hot-pressing, should help retain a homogeneous coating as well as being thin for easy peel of after hot-pressing (35).

## 2.5 Methods of Analysis

The following sections describes the methods of analysis used to determine the catalyst ink rheological properties and final electrode performance.

### 2.5.1 Rheological Measurements

Rheology is defined as the study of the deformations and flow of matter as a result from the application of a force (36). Numerous scientific disciplines use rheology to determine the properties and behavior for different materials. The intermolecular forces of the material is what determines the physical response to the applied stress, but the timescale can also strongly influence the rheological measurements. Two different timescales for the same experiment might yield two very different results. This is because the structure of the material is a result of both the force and the timescale for changes in the microstructure. A material will deform as a result of an applied stress, where the relative deformation, or deformation per unit length is defined as the strain. The shear strain is produced by the application of a shear stress, $\sigma$. When a force is applied on a fluid, the fluid will move until the stress is removed. For a liquid between two surfaces separated by a small gap, illustrated in Figure 2.8, a constant sheer stress is required to move the upper surface at a constant velocity, $u$. If there is no slip between the surface and the liquid, then the

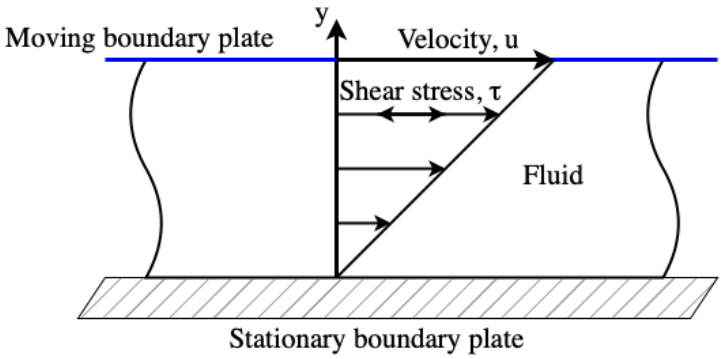


**Figure 2.8:** The Figure illustrates the shear stress on a fluid as a result of the moving upper plate.

velocity of the liquid will continuously change from u at the upper surface to zero at the lower surface. For every second the displacement produced is x and the strain is:

$$\gamma = \frac{x}{z} \tag{2.5}$$

the velocity can be written as $u = dx/dt$, hence the rate of strain, or here called the shear rate is

$$\frac{\mathrm{d}\gamma}{\mathrm{d}t} = \frac{u}{z} \tag{2.6}$$

For large gaps the shear rate changes across the gap so the equation is instead written as:

$$\dot{\gamma} = \frac{\mathrm{d}u}{\mathrm{d}z} \tag{2.7}$$

When the plot of shear stress versus shear rate results in a linear curve the liquid is Newtonian, but the range at which this behaviour is observed is very limited and non-linear behavior is often observed. For catalyst inks the rheological behavior is far more complex.

Rheological measurements makes it possible to quantitatively determine the bulk microstructure of catalyst inks as the rheological properties of inks are very sensitive to changes in the microstructure. The microstructure of the ink are controlled by the interactions between Pt, CB, ionomer and solvent. The rheological properties of catalyst inks are important as it determines how the inks behave during fabrication of CLs (37). Different processing and coating methods will result in different stresses on the ink, hence will the rheological properties strongly influence the characteristic of the ink and the final electrode. Rheological measurements can also be used for process optimization and quality control (2). There is several studies investigating the microstructure of carbon black dispersions and ionomer solutions but few studies reports on the rheology of dispersion containing both Pt on CB and ionomer.

In this thesis, shear viscosity and shear modulus are investigated to correlate the rheological properties to the degree of dispersion of the inks. A well dispersed ink should have a higher interaction between catalyst and ionomer, which should give a higher viscosity compared to a poorly dispersed ink with big carbon agglomerates. To achieve good coatings with the doctor blade, a shear thinning behaviour is desirable as well as relatively high viscosity. If the viscosity is too high, then the ink will not flow with the doctor blade and will not coat the decal (33). Still, the viscosity should not be to low so that the ink flows too easily and in undesired direction when coating. Thus, a shear-thinning behaviour is preferred, as it allows for good control of the ink while the ink in the coating direction becomes shear thinned and can be easily coated. To describe the viscoelastic behavior of the ink, the complex shear modulus is analyzed. From the complex shear modulus can the storage modulus (G') and loss modulus (G") be obtained that represent the elastic and viscous portion of the viscoelastic behavior. The viscous behavior arise from the friction between the ink components and the energy becomes dissipated, meaning it is no longer available for further behavior of the ink (38). The elastic portion of energy is stored in the ink without destroying the structure of the ink so when the force is removed, the stored energy act as a driving force to reform the ink to its original shape. To achieve reproducible electrodes, the ink should not change shape or structure when handling after coating. Hence is it important for the ink to have a higher storage modulus (elastic component) than loss modulus (viscous component). The desirable shear modulus behavior is relatively high values with the storage modulus being ten times higher then the loss modulus up until at least a complex shear stress of one Pa. This is based on the forces involved in the coating process of the electrodes.

### 2.5.2 Single Cell Measurements

A single PEM fuel cell is made up of only one anode and one cathode, meaning the operating voltage is less then 1 V, but the voltage is even less when operating under a specific current. A modern single cell have a performance of at least 1 $A/cm^2$ at a voltage of 0.6 V. This makes it possible to detect small changes in operating voltages when doing single cell measurements. This in turn allows for measuring the effect of changes in the electrode microstructure, as small changes in the microstructure might influence the operating voltage. A potential problem that PEM fuel cell development might face is being tricked by the begging of life performance. Most electrodes perform very well in the begging of their life, but electrodes of poorer quality will over time decrease in efficiency. The reason for this is agglomeration and Ostwald ripening of the Pt particles as well as degradation of the membranes. By performing single-cell measurements in different operating conditions, the electrode performance at beginning of life can be measured quicker and more easily as compered full-stack tests.

# 3
# Methods

## 3.1 Materials Overview and Sample Preparation

The Pt/CB catalysts and pure carbon support used consisted of two different Pt on HSC support, one Pt on GC support and one pure HSC powder. The Pt on HSC support, called HCE and HCK, have a platinum loading of 47wt.% and 52wt.% respectively. The Pt on GC support, called GCE, have a loading of 50%. The catalyst inks were prepared by mixing desired amount of Pt/CB or carbon powder with water, followed by ionomer and 1-propanol. Two different ionomers were investigated, one short side chained ionomer and one long side chained ionomer, called SSC and LSC respectively. Each ink is made with a ionomer to Pt weight percent ratio of one, except for the inks with carbon powder were the ionomer to support weight percent ratio of one was used. The dry weight percentage is defined as the sum of Pt, CB and dry ionomer, and a value of 12,6% was used. The solvent matrix consists of Milli-Q water and 1-propanol to a ratio of 40:60. The ionomers used are pre-dissolved in either only water or a mixture of water and 1-propanol. This solvent is counted for when the additional solvent matrix is added, resulting in the total amount of solvent to be water and 1-propanol with a ration of 40:60.

The Pt/CB or carbon powder was weight into a vial to the desired amount and the scale was then zeroed. This was followed by adding water in the same vial until the right weight was reached and the process was repeated with ionomer and 1-propanol. This sequence of adding the components are important as the Pt/CB is highly reactive with alcohol and could combust if 1-propanol was added before the Pt/CB was thoroughly wetted. When all components had been added the lid was screwed on and the vial was shaken by hand to ensure that the components were mixed. A magnetic stir bar is then added and the vial is placed on a magnetic stirrer plate for maturation over night, or longer, at 350 rpm.

## 3.2 Ultrasonic Dispersion of Catalyst Inks

The tool used for ultrasonic dispersion of the catalyst ink was a stand mounted ultrasonic probe device. A sonotrode with a diameter of 22 mm was used. With the software belonging to ultrasonic device, the amplitude of the sonotrode, the energy input limit, time limit and more can be defined. The software also shows live data during the dispersion of the total energy input in watt-seconds or kilowatt-hours, as well as the momentary input in energy from the sonotrode (Power tot.) and the

amount that have been absorbed by the sample (Power net.). A common problem when dispersing a sample in a vial is that the vial moves due to the vibration so that the neck of the vial comes in contact with the sonotrode, this leads to the energy going to the vial which heats up quickly. When this happens the Power net. drops, so by monitoring the energy input this can be avoided. The sonotrode is calibrated in air prior to every new sample.

The inks were either dispersed in the same vial that the ink had been mixed in, or by pouring the ink into a so called flow cell. For the first alternative, the vial was put in a water bath with cold water and then placed on a platform under the sonotrode that can be moved up and down. For later experiments, a magnetic stirrer plate was also added under the water bath to ensure good mixing of the ink. When the sample is ready, the platform is raised until the sonotrode is emerged in the ink, without touching with the vial. A thermometer connected to the sonotrode software was placed in the water bath to monitor the increase in temperature of the water during dispersion. If the temperature increased above 35°C, the dispersion was interrupted and the water was changed for colder water.

For the flow cell, the ink is poured from a beaker into the cell. The flow cell is a jacketed vessel in stainless steel which allows for cooling liquid around the inner department where the ink is dispersed. The flow cell ensures that the ink never overheats during dispersion. A picture of the flow cell and a schematic figure is shown in Figure 3.1. A recirculating cooler was used to pump cooled water around the flow cell. With the flow cell, the ink is also pump through the vessel to ensure that the ink is being well dispersed and cooled. To not contaminate the pump or ink, a peristaltic pump system was used. The pump work by compressing the flexible tube while rotating, forcing the fluid to move through the tube. After the ink was poured into the flow cell, it was made sure that the cooling water had reached the right temperature. Then the cell was raised to immerse the sonotrode and the peristaltic pump was set to 200 rpm.

The inks dispersed without the flow cell was placed in a water bath at around 20°C and was then dispersed with amplitude of either 20% or 50% until the desired energy input was reached. The sonotrode was placed so that it did not touch the vial to prevent loss in energy input due to transfer to the vial. However, during the dispersion, the vibrations made the vial move and temporarily the power dropped due to the sonotrode being in contact with the vial. To prevent overheating the sample, a thermostat was placed in the water bath to monitor the warming of the sample and cooling water. It was predetermined that a temperature of 35°C of the cooling water was a critical value, correlating that the ink might be damaged by the heat. In the software to the ultrasonic device the exact energy input is denoted meaning that the ink is dispersed to exactly that value. After dispersion the ink was placed on the magnetic stirrer again to erase any loading history of the microstructure for 30 minutes before coating and rheology measurements.

The ink that was dispersed with the flow cell was first mixed in a beaker and then

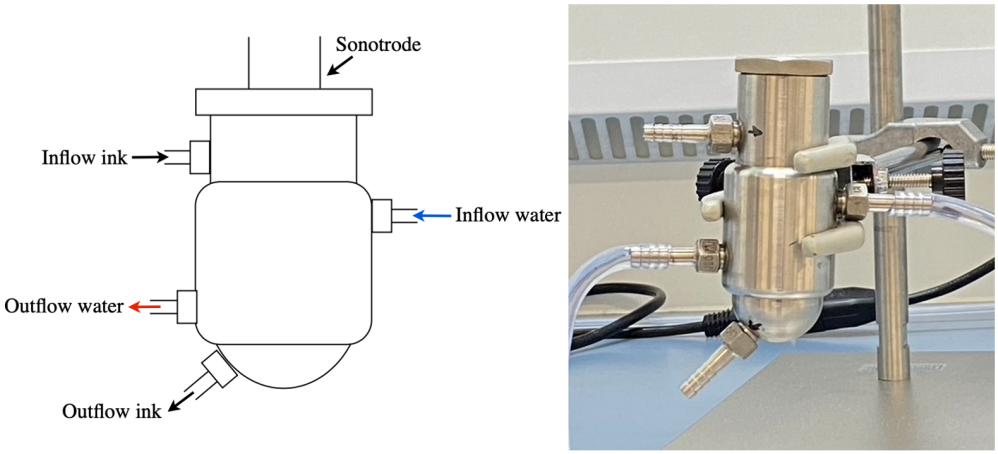


**Figure 3.1:** A schematic figure of the flow cell showing the in- and outflow of ink and cooling water, as well as a picture of the flow cell used.

poured into the flow cell after maturation. The recirculating cooler was put to 10°C to ensure that the ink was kept at low temperature and the peristaltic pump was turned on as soon as the ink was poured in. The ink was dispersed with an amplitude of 50% up until the determined energy input was reached. With the flow cell the ink was not put on the magnetic stirrer to erase the loading history on the microstructure as it would result in a great loss of ink sticking to the beaker walls and so on. Instead the ink was kept in the flow cell with the peristaltic pump mixing the ink at a low setting and the recirculating cooler was increase to 20°C. After 30 minutes the peristaltic pump was turned off and the flow cell was lowered to be able to pipette out a few milliliters of ink for rheological measurements and coatings.

When the dispersion was complete, the tube for inlet flow of ink was detached and the ink was then pumped into a beaker. The flow cell was cleaned by reattaching the inlet flow tube to the flow cell, pumping water through the flow cell for a few minutes, then emptying the water in a waste bucket and repeating with a 50:50 water and 1-propanol mixture. This procedure was repeated until the flow cell was clean. The flexible tubes for the peristaltic pump was difficult to clean so to avoid contamination, the same tube was only used for recipes containing the same catalyst and ionomer.

## 3.3 Rheological Measurements

To determine the rheological properties of the ink and the effect of dispersion on the rheology a rheometer was used. A cone-plate geometry with a 4° angle and 40 mm diameter was used for all measurements. The sequence consists of three runs, where each run starts with viscometry measurements followed by oscillation amplitude measurements. The viscometry measurements runs a table of shear rate between 0 and $10^3$ $s^{-1}$ while measuring the torque resulting in a Viscosity versus Shear rate graph. The oscillating amplitude measurements runs a table of amplitudes from the

start stress 0.010 Pa to the end stress 100.0 Pa logarithmic taking five samples per decade, resulting in a graph showing Elastic modulus, Viscous modulus and Phase angle versus Shear stain. The rheometer is connected to a heat exchanger that circulates fluid adjacent to the plate, allowing for the measurements to be taken at exactly 25°C.

Rheological measurements were taken for all inks before dispersion to see if any slight difference in recipe or time for maturation could have any affect of the properties of the ink. If two ink of the same recipe show the same rheological properties undispersed, then it can conclude with greater certainty that any later difference in rheological properties between the samples are due to the difference in dispersion methodology.

1,4 ml of the ink was pipette onto the plate and the cone was lowered. The sample was investigated to make sure that the right amount of ink was loaded. The ink should cover the cone without pouring over the edges. A slight bulge should be seen between the cone and plate. If a too small amount of ink was loaded the cone is elevated again and more ink can be loaded. If too much ink is loaded onto the plate the cone will push the excess out to the side when being lowered and the excess ink can be trimmed off. After loading the sample, solvent in the form of 1-propanol is loaded into the solvent wells and the solvent trap is mounted. The solvent trap prevent the solvent in the sample to evaporate. After loading the rheometer with the a sample of the dispersed ink, the rest of the ink is dispersed and matured for 30 minutes, followed by further rheological measurements. This process is repeated for all the differently dispersed inks. After the measurements are finished the ink is cleaned of by paper wipes and alcohol wipes leaving a clean surface ready for the next experiment.

## 3.4 Doctor Blade Coating

For light microscope analysis and the fabrication of MEAs for the single-cell tests, the catalyst ink needs to be coated onto decals. The coatings of ink onto decals were produced using the doctor blade method. The doctor blade method is used for its preciseness in catalyst loading and high reproducibility and because it is easy to use. The doctor blade consists of a stainless steel adjustable blade in between two smooth and flat stainless steel blocks. The blade can be raised or lowered along these blocks with micrometer precision. The height can be adjusted by turning a wheel and that then is locked into place to avoid that the height changes during coating. The bottom of the blade has a slight angle creating a blunt edge. Complementing to the doctor blade is the film applicator that pushes the doctor blade forward, shown in Fig. 3.3. The coating surface of the film applicator consists of a vacuum suction plate. The plate have circular suction areas of 25 mm diameters of sintered metal and is connected to a vacuum pump. The decal is held in place by clamps attached to the film applicator and is held flat to the surface due to the suction. After the decal has been put in place and the doctor blade has been placed in front of the applicator, the ink is placed in a line in front of the blade with a pipette. The

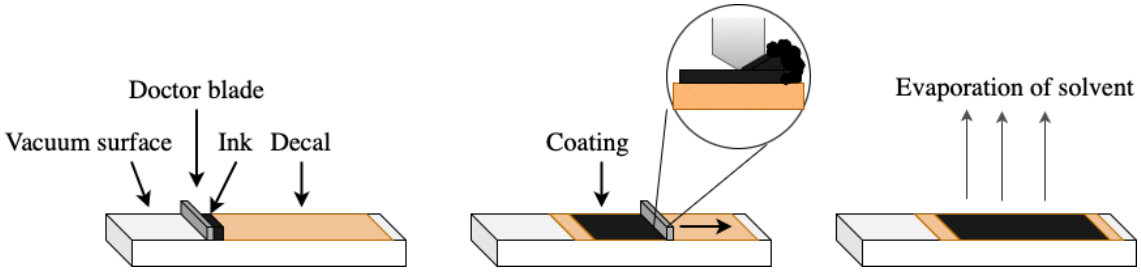


**Figure 3.2:** The Figure shows the process of coating with the doctor blade method.

**Figure 3.3:** Picture taken of the doctor blade coater.

applicator then pushes the blade from behind at a constant speed over the decal, dragging the ink along. Left behind the doctor blade is a film of ink with the same height as the so called gap height, the distance between the doctor blade and the decal. The mechanism of the doctor blade coating is showed schematically in Figure 3.2. The distance from the blade to the decal can be varied from 0 to 900 $\mu$m and the coating speed can be varied between 10 and 107 mm/s.

Coatings for investigation under the light microscope were made with two different gap heights, 50 $\mu$m and 200 $\mu$m. The purpose of the 50 $\mu$m coatings was to give a better view of the agglomerates in the ink, as a thinner coating would allow less agglomerates to be covered by the bulk ink. The 200 $\mu$m thick coatings were of interest because that gap height results in a desired loading of Pt in cathode prototypes, but it is usually difficult to obtain such a thick coating without crack formation. Hence was coating made with that gap height to investigate the effect of dispersion parameters on thicker coatings. Coatings made for single-cell testing were made with 100 $\mu$m gap height because of standard Pt loading requirements. All coatings were made with the doctor blade. The decal was cut into 20x25 cm pieces and then clamped to the film applicator. The vacuum pump was switched on and the doctor blade was put in place. The 50 $\mu$m coatings were made by pipette around 1 ml of ink in front of the blade and then coat with a speed of 20 mm/s. The 200 $\mu$m coating was made in the same way but with 2-3 ml of ink. The ink used for coating were taken straight from the magnetic stirrer after maturation if it had been dispersed in a vial. If it had been dispersed in the flow call, the ink

were taken straight from there after it had been matured. After coating the clamps are loosened and the decals were slid onto plastic sheets and carefully transferred to the drying station. The drying station consist of a light label and a plexiglass box. The light table is used to inspect bigger cracks in the coating as they light up when a strong light shine from behind. The plexiglass box is placed over the coating to retain the evaporated solvent in the atmosphere around the coating. This is done to prevent crack formation. The coating were left to dry for at least three hours or up to a day.

## 3.5 Light Microscopy

A digital light microscope is used to investigate the produced coatings. The microscope creates a magnified image by the use of a series of glass lenses (39). A beam of light is focused on the sample and a convex objective lens then enlarge the formed image. Unlike a traditional microscope, the digital microscope do not have eyepieces. Instead, a camera acts as detector the image is displayed on a monitor. There are three objectives to the microscope, one low, one mid and one high magnification objective. A high magnification objective was used with a field of view of 3.60 mm and a magnification up to 2350x. A transmitted light insert on the stage of the microscope was used to detect small cracks in the coatings that are otherwise invisible. A ring light integrated in the objective and a coaxial light integrated in the tilting stand were also used. The intensity of all three light sources was controlled with the belonging software. With the software it is also possible to change the exposure time of the camera and increase the grain. Beyond regular 2D imaging, the software contains a function called Z-stacking. The function stacks pictures in the z-direction and the software can then calculate the 3D profile from these pictures. This enables for several measurements, such as measuring the diameter of big agglomerates that is located on the surface of the coatings. It also makes it possible to determine is a surface that appears flat really is that, and if not, the height difference can be determined. The microscope pictures enables for a quick way to determine if a coating contains any big cracks or if it looks homogeneous.

The 50 $\mu$m and 200 $\mu$m coatings were investigated under the light microscope after they had been completely dried. The coating was placed under the microscope and the stage was raised until focus was found. Once the coating was in focus, the magnification was increased to 200x and focus was adjusted again. As the microscope was placed on a regular table, slight shaking of the table could cause blurry images. To avoid this, the ring light intensity was decreased a few percent and the exposure time was increased to up to 300 ms, for more sharp images. Before any images were taken, several parts of the coating were investigated to make sure that the part that was being photographed was a fair representation of the coating. The back light was also switched on and off to see if any cracks were present, and that would then light up if that was the case. The centre of the coating was if most interest but the edges were also investigated. A scale bar was water stamped onto all images to make comparison easier. Once a satisfactory amount of images at 200x was taken, the magnification was increased to 500x and the process was repeated. If any structure

**Figure 3.4:** Picture taken of the light microscope where the transmitted light insert on can be seen attached on the stage.

of special interest was found, it was looked at with further magnification.

For coatings that was not cracked but showed distinct agglomerates, the z-stack function was used. First, the magnification was increased to 1000–1200x depending on the agglomerate size. To determine the number of pictures that should stacked to achieve a good 3D representation of the surface, the depth of the surface needs to be determined. This is done by first setting the focus just above the top of the agglomerate, the part closes to the microscope, and locking it in the software. Then the stage is carefully raised, going beyond when the coating is in focus up until the part furthers from the microscope is out of focus. This is locked into the software and the number of images needed is calculated. The z-stacking is then initiated and the microscope starts by taking the first picture out of focus, moving the stage so the part furthest from the microscope is more in focus and taking one more image. This procedure is repeated for as many images that was calculated to be needed. The result is a sharp image of the 3D surface where all parts are in focus and the unevenness of the coating is calculated.

## 3.6 Preparation for In-situ Testing

For the single-cell testing, the electrodes needs to be assembled into MEAs. To produce the MEAs the cathode and anode has to first be coated onto decals using the doctor blade. The coating and drying of the electrode was done in a climate controlled room. The cathode is made from a ink with HCE catalysts and SSC ionomer and is coated with a wet height of 100 $\mu$m and with a speed of 20 mm/s. The anode was made from an ink with GCE catalyst and SSC ionomer and was coated with a wet height of 30 $\mu$m and a speed of 20 mm/s. After coating the inks they were transferred from the vacuum surface to the drying station where they are

put under plexiglass boxes do dry under more regulated conditions. After drying was the electrodes assembled to MEAs by hot-pressing. A cathode and an anode was placed on each side of a membrane and then hot-pressed at 180 °C with 450 $N/cm^2$ for 300s. The MEAs was then cut and added to a sub gasket.

## 3.7 In-situ Testing

In-situ testing was performed during normal, hot and warm-up operating conditions to obtain polarization curves and cyclic voltammetry (CV) measurements were made for insight in ECSA, capacitance layer, hydrogen crossover, internal resistance and roughness factor. Before measurements was the MEA conditioned for 12 hours and then CV measurements was made under dry conditions with a relative humidity of 25% in the inlet gas. After CV measurements was normal condition polarization tested, followed by CV measurements with a relative humidity of 100%. Normal conditions was then tested again, giving two measurement for normal condition with MEAs that had been exposed to different relative humidity prior to measurement, to obtain information of how much ionomer is in contact with the catalyst. This was then followed by polarization measurements during hot and warm-up conditions. The difference between normal, hot and warm up conditions is the coolant inlet temperature that is 45°C for warm up, 65°C for normal and 85°C for hot. The relative humidity is also influenced by the different temperatures of the coolant. CV measurements are not presented in the result part due to difficulties interpreting the results and limited time.

# 4

# Results

The following chapter presents the rheological findings of the catalyst inks and discussion behind the underlying interactions of the ink microstructure. Micrographs of the produced electrodes are presented to correlate the rheological behavior of the inks with electrode surface characteristics. In-situ testing was performed for some electrodes to investigated the electrode performance. Due to the complexity of the catalyst inks, a systematic investigation of the ink components and dispersion parameters have been performed. Two HSAC supported and one GC supported Pt catalysts, KB 3000 carbon support, SSC and LSC ionomers have been investigated for different ultrasonication vibration amplitude, total energy input, ultrasonication setup and the effect of bead-milling.

## 4.1 Effects of Ultrasonication Amplitude

The first part of this study consisted of deciding the effect of vibrational amplitude of the sonotrode during dispersion. The choice of amplitude settings was based on earlier findings from the lab while still taking sonotrode probe diameter differences in consideration. An amplitude of 20% was set as a typical low value and a maximum amplitude of 50% was chosen to avoid excessive splashing and overheating the ink sample when sonicating. To investigate the effect of vibrational amplitude, the ink samples was dispersed to 10 and 50 kWs in a vial with a sonotrode amplitude off either 20% or 50 % and the effect of different amplitudes was investigated for the two different energy inputs.

### 4.1.1 HCE Catalyst and SSC Ionomer

The viscosity and modulus rheological measurements of ink samples containing HCE catalyst and SSC ionomer dispersed to 50 kWs with either 20% or 50% amplitude are presented in Fig. 4.1. Both sample show a decrease in viscosity with increasing shear rate. The ink dispersed with an amplitude of 50% show a slightly higher viscosity compared to the sample dispersed with 20% amplitude. The modulus curve show that the shear modulus of the sample dispersed with 50% amplitude is slightly higher than the other sample and does not decrease as fast when the complex shear stress approaches one Pa.

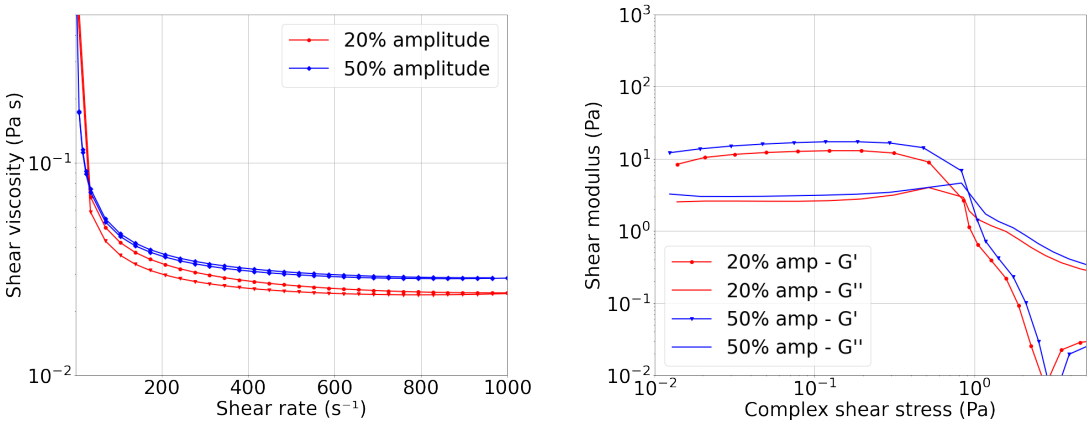


**(a)** Viscosity curves **(b)** Modulus curves

**Figure 4.1:** Rheological properties for ink with HCE catalyst and SSC ionomer dispersed with 20% and 50% vibrational amplitude. In the modulus curve is the elastic component presented as G' and the viscous component as G"

Micrographs of electrodes coated from the two ink dispersions with a gap height of 50 $\mu$m are shown in Fig. 4.2. Both coatings show apparent agglomerates but the ink dispersed with 50% amplitude show fewer and smaller ones. Measurements with the microscope software showed that the diameter of the agglomerates are almost halved from 19$\mu$m to 10,5$\mu$m by increasing the amplitude from 20% to 50%. Micrographs of the electrodes made with 200 $\mu$m gap height, presented in Appendix B.1, show severely cracked structures and no apparent difference between the amplitudes.

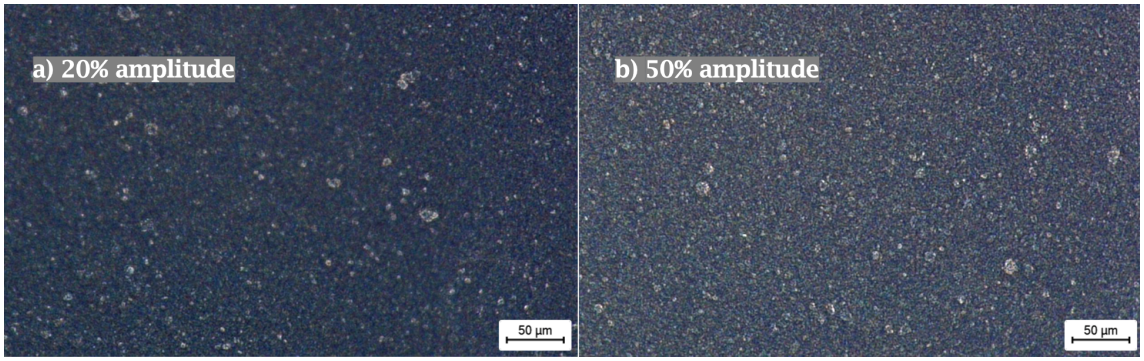


**Figure 4.2:** Micrographs with 500x magnification of coatings made with the ink containing HCE catalyst ans SSC ionomer dispersed with 20% amplitude (a) and with 50% amplitude (b).

These results suggest that there is an effect from vibrational amplitude on the microstructure of the ink. According to Pollet (29) is the ultrasonic intensity proportional to the vibrational amplitude squared, and that an increase in ultrasonic intensity will lead to an increase in sonochemical effects. The higher amplitude can be seen to decrease the agglomerate size which would increase the interactions between the agglomerates and ionomer due to the increased surface area, which in turn

would increase the viscosity and modulus of the ink. It should be noted that the largest agglomerates presented here are the ones found on the surface after coating and that agglomerates can be hidden in the bulk of the coating. It is also possible that agglomerates at the surface can be broken up by the shearing forces of the doctor blade when coating. How well the surface of the coating corresponding to the electrode bulk is not well investigated for samples with this high solid content. Because of the complex forces that occur when the electrode dries it could be possible that larger agglomerates migrates to the surface and hence is the surface not a fair representation of the bulk. When scanning the surface with the z-stack function, it was found that the height of the agglomerate above the surface was less than the width. For the sample with the 10.50 $\mu$m wide agglomerate, it was found that the deviation from the surface height was only 1 $\mu$m. This could indicate that only a small part of a larger agglomerate is visible but could also be due to the software function not being used correctly. With light microscopy only the surface can be viewed but Bapat et. al. (2) used transmission electron microscopy (TEM) micrograph to image ink dispersion, allowing to see straight through the sample. TEM allows for characterization with high resolution but requires excessive dilution which might alter the microstructure of the ink dispersion. Dynamic light scattering (DLS) has also been a reported method in litterateur to investigate agglomerates, but DLS also requires dilute solutions. It was reasoned for this work that the dilution of ink dispersion would alter the microstructure and interaction between components to the degree where the results from TEM or DLS would not be corresponding to the agglomerated structures in the undiluted ink, and hence would not give insight in the effects of dispersion methodology on agglomerate structure. Scanning electron microscopy (SEM) is a third possible analyzing tool that can be used to analyze the CL surface directly and have seen used in several studies (40). SEM was not used in this theses due to time limitations.

### 4.1.2 HCK Catalyst, KB 3000 and SSC Ionomer

Further experiments were made to investigate the effect of sonotrode amplitude on different ink components. The purpose was to investigate the effect the different catalyst has during dispersion of the ink with different amplitudes and compare the resulting rheology and electrode appearance between catalysts. A comparison between HCE and HCK was made to see the effect on two different HSAC catalysts and the results was also compared with pure KB 3000 carbon support to see what effect the Pt has on the dispersion of the inks.

The rheological measurements for the ink containing HCK catalyst and SSC ionomer, presented in Appendix B.2, showed a very low viscosity with Newtonian behavior for the sample dispersed with an amplitude of 20%. The ink dispersed with 50% showed low viscosity and Newtonian behaviour for the first shear rate run, but the sample then splashed out from under the rheometer cone making the rest of the measurements invalid. The modulus curves for both samples showed poor rheological behavior with very low elastic and viscous modulus. Micrographs of coatings

made from the inks with a gap height of 50 and 200 $\mu$m are presented in Fig. 4.3. It is visible from the coatings that the amplitude have had an effect of the agglomerate size. The coatings made from the ink dispersed with 50% amplitude exhibit smaller agglomerates and no crack formation for the 200 $\mu$m thick coating as compared to the respective coating from the ink dispersed with 20% amplitude.

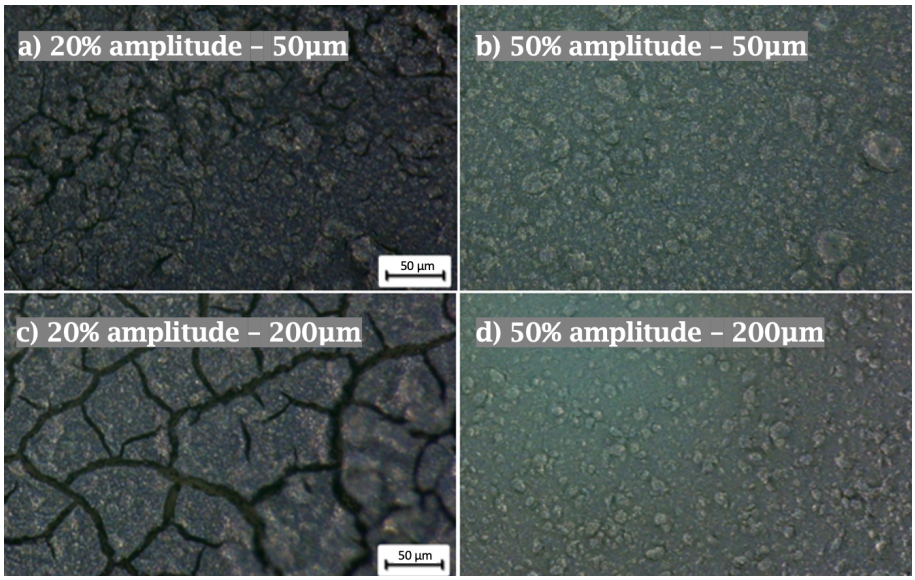


**Figure 4.3:** Micrographs of 50 $\mu$m and 200 $\mu$m thick coatings of ink with HCK catalyst and SSC ionomer dispersed with either 20% or 50% amplitude. Micrographs a,b and c are taken with 500x magnification while d is taken with 200x magnification. Scale bars for b and c was not available.

The rheological measurements for the ink containing carbon support KB 3000 and SSC ionomer are presented in Fig. 4.4. The samples show a shear thinning behavior, high viscosity and low modulus values. The ink dispersed with 50% amplitude show a higher viscosity and modulus curve compered to the ink dispersed with 20% amplitude.

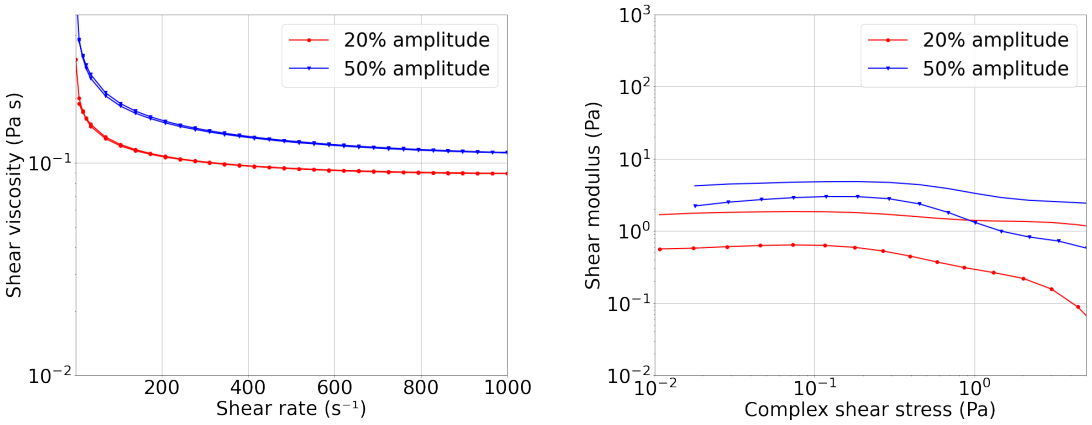


**(a)** Viscosity curves **(b)** Modulus curves

**Figure 4.4:** Rheological measurements of the ink with KB 3000 and SSC ionomer dispersed to 50 kWs with vibrational amplitude of 20% and 50%.

Micrographs of electrodes made with a gap height of 50 and 200 $\mu$m form the inks dispersed with 20% and 50% amplitude are presented in Appendix B.3. The electrodes made with 50 $\mu$m gap height showed the same trend as the previous sample, with a significant decrease in both agglomerate size and abundance with increased amplitude. The electrodes made with a gap height of 200 $\mu$m showed severely cracked structures and the ink dispersed with 50% amplitude exhibit the largest cracks.

The reason behind the undesired rheological properties for the ink containing HCK catalyst and SSC ionomer is probably not because of poor dispersion and more likely a result of a poor choice of solvent matrix and ionomer for this kind of catalyst that would need a different ink components or a higher solid content. Because of the failed rheological measurements, it is not possible to draw any conclusions regarding the effect of sonication amplitude on the rheological properties. The effect of amplitude can however be seen in the coatings, where the ink dispersed with 50% show significantly smaller agglomerates compared to the ink dispersed with 20% amplitude. The visible effect is even grater than for the ink containing HCE catalyst. The ink containing KB 3000 and SSC ionomer show a generally higher viscosity than the ink containing HCE catalyst and SSC ionomer which is due to the pure carbon having both a higher internal porosity and a more agglomerated structure. The solid content for the ink with KB 3000 and SSC ionomer was 12.5% and 12.6% respectively were the solid content is the sum of weight percentage of the solid components (ionomer, carbon and/or platinum). This small difference in solid content would not give rise to the large difference viscosity between the two inks. The reason is probably that the ink with KB 3000 has in practice twice the amount of internal pore volume of carbon particles as compared to the catalyst HCE and that the Pt on the catalyst provide stabilisation via electrostatic repulsion.

## 4.2 Effects of Ultrasonication Energy Input

To further investigate effect of the total energy input on the ink dispersion and then electrodes, both microscopy, rheological measurements and in-situ testing was used. Inks were investigated when undispersed and dispersed to different total energy inputs to investigate the effect on the microstructure.

### 4.2.1 HCE Catalyst and SSC Ionomer

The rheological measurements for ink with HCE catalyst and SSC ionomer are presented in Fig. 4.5 for samples undispersed and dispersed to 10, 50, 100 and 200 kWs. The viscosity curves show an increase in viscosity with increasing dispersion energy up to 100 kWs where the viscosity for the ink dispersed to 200 kWs show a lower viscosity compared to 50 and 100 kWs dispersed inks. The temperature of the ink after being dispersed from 100 to 200 kWs was 62°C. The undispersed and 10 kWs dispersed sample show different viscosity for increasing and decreasing shear rates, with an initially higher viscosity that decreases with the decreasing shear rate. The higher dispersed inks do not show the same behavior. The shear modulus measurements presented in Fig. 4.5b show similar properties for inks dispersed to 50, 100 and 200 kWs while the undispersed ink and the ink dispersed to 10 kWs show much lower shear modulus. The undispersed ink show a lower elastic component than viscous component of the shear modulus while the opposite is true for the other inks. The inks dispersed to 50, 100 and 200 kWs show a shear modulus behavior that is desired based on a handing point of view in this work.

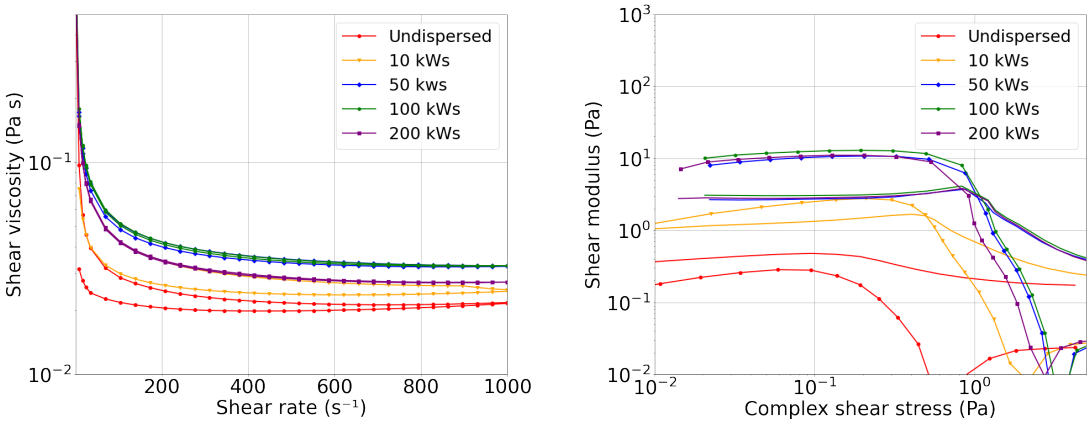


**(a)** Viscosity curves **(b)** Modulus curves

**Figure 4.5:** Rheological measurements of an ink with HCE catalyst and SSC ionomer undispersed and dispersed to 10, 50, 100 and 200 kWs.

The difference in viscosity for increasing and descending shear rate is commonly observed with ionomers and is probably because the ionomer chains prior to shearing are intertwined in a network. When a shearing force is applied, the chains start

to disentangle, making it easier for the chains to flow past each other and hence decreases the viscosity. The time it then takes for the chains to entangle again is less the time the ink is being sheared, resulting in different viscosity. The behaviour is only present for the inks that are less dispersed, suggesting low interaction between catalyst and ionomer and a more intertwined ionomer network. The highly dispersed ink do not show the same behavior suggesting that the inks have smaller agglomerates that can interacts more with the ionomer, changing the shear thinning behavior otherwise shown.

Micrographs of the electrodes of ink with HCE catalyst and SSC ionomer undispersed and dispersed to 50, 100 and 200 kWs with a gap height of 50 $\mu$m are presented in Fig. 4.6. The micrographs show that the visible agglomerates decrease in size with increasing dispersion energy. The most significant decrease in agglomerate size can be seen between the undispersed sample and the one dispersed to 50 kWs. Measurements taken of the largest agglomerates for each coating show that the size of the agglomerates is 132, 18, 16 and 9 $\mu$m for the undispersed, 50, 100 and 200 kWs coatings, respectively.

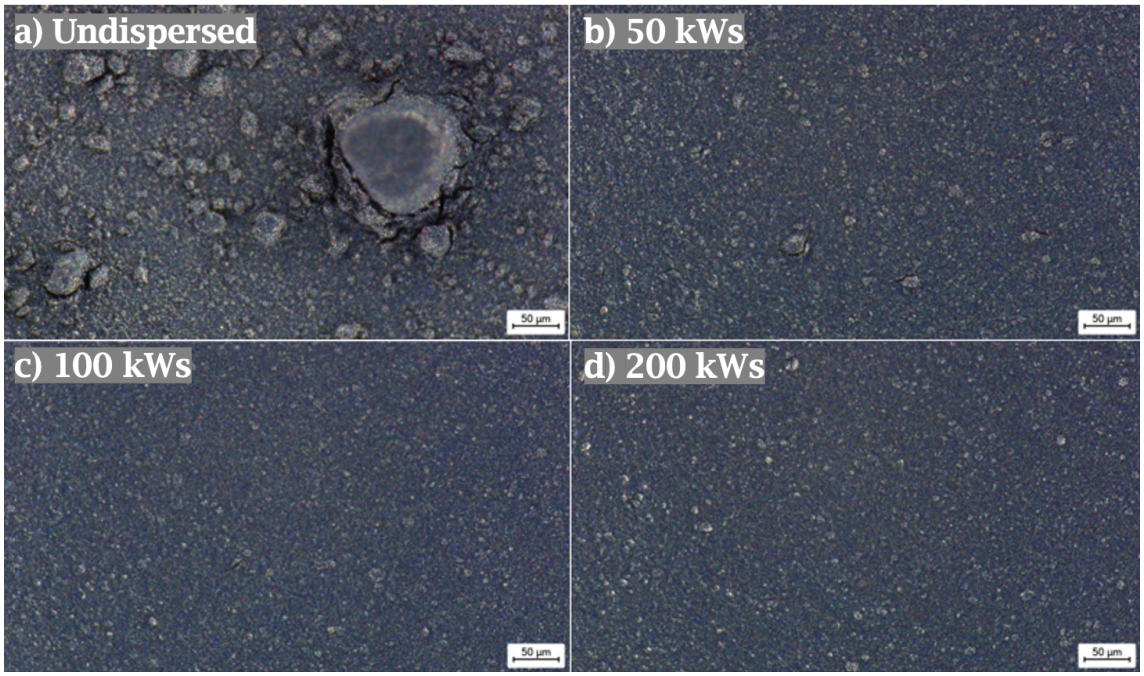


**Figure 4.6:** Micrographs with 500x magnification of 50 $\mu$m thick coatings of ink with HCE catalyst and SSC ionomer left undispersed and dispersed to 50, 100 and 200 kWs.

Micrographs of electrodes made with 200 $\mu$m gap height are presented in Appendix B.4. The undispersed coating show large agglomerates and crack formation especially around the agglomerates while the coatings from the dispersed inks all exhibit larger and more regular cracks. The coatings made from the inks dispersed to 50 and 200 kWs show wide cracks with chunks of coating well separated, forming a tessellated structure. The individual tiles for the 200 kWs coating are larger then for the

50 kWs coating. The coating from the 100 kWs dispersed ink show less wide cracks. It was expected that a more well dispersed and homogeneous structure would be more enduring to the stresses forming in the coating when the solvent evaporates, and hence be more crack resistant. The micrographs shows that the sizes of the cracks increase with increased degree of dispersion. Even though the cracks for the more well dispersed coatings are larger and wider, the amount of cracks are fewer. The less dispersed ink have a less homogeneous microstructure with more defect where cracks can start to form. Although the more dispersed ink have fewer defect, some are still present for cracks to form at. The amount of solvent evaporated for all coatings are the same so the volume of the coating will decrease the same. When cracks are formed, the tiles will keep decreasing as the rest of the solvent evaporates and the wider gaps between the tiles will form.

To investigate whether the ultrasonic energy input would have an effect on the electrode performance, MEAs was made from different dispersed electrodes and then tested in-situ. A coating with the undispersed sample was initially made for testing but after drying it was assessed that the large agglomerates and very rough surface structure would result in bad transfer of the electrode to the membrane. A coating made with the ink dispersed to 10 kWs was instead made to represent a poorly dispersed electrode. Coatings made from the inks dispersed to 50 and 200 kWs was made to represent medium and highly dispersed electrodes. These electrodes was made with a gap height of 100 $\mu$m resulting in a loading of 0.25 mg/cm$^2$ and was used as the cathodes in the MEA. The anodes were made from an ink containing GCE catalyst and SSC ionomer dispersed to 200 kWs and coated with a gap height of 40 $\mu$m resulting in a loading of 0.1 mg/cm$^2$. Rheological results and micrographs of the ink used for the anodes are presented in Section 4.2.3. The produced MEAs were tested in normal, hot and warm up operating conditions. The polarization curves for the MEA produced with the electrode made with the ink dispersed to 10 kWs tested in normal, hot and warm up conditions are presented in Fig. 4.7.

Data points are shown for the normal operating conditions (NOC2). The open circuit voltage can be seen to be 0.954 V at 0 A/cm$^2$. The ideal case would have 1.23 V but due to hydrogen crossover the value is lower. At 0.1 A/cm$^2$ the cell voltage is 0.866 V, here the activation losses are dominant. The further decrease of the polarization curve after this point is due to ohmic losses and it can be seen that the curve decreases linearly to 2.5 A/cm$^2$ meaning that there is no mass transport losses. The curve displays a final voltage of 0.585 V at 2.5 A/cm$^2$. For hot operating conditions (HOT), the open circuit voltage is 0.948 V. At 0.1 A/cm$^2$ the cell voltage is 0.86V and the curve can be seen to decrease very similarly to the NOC2 curve up to 1.5 A/cm$^2$. The voltage then drop to 0.6 V at 1.9 A/cm$^2$ attributed to mass transport losses. The hot operating condition is limited to maximum current density of 1.9 A/cm$^2$ which is why there are no data points past this value. The open circuit voltage for the warm-up operating condition (WUP) is 0.948 V and at 0.1 A/cm$^2$ the cell voltage is 0.85 V. The mass transport losses are greater under these conditions resulting in a cell voltage of 0.507 V at 2.5 A/cm$^2$.

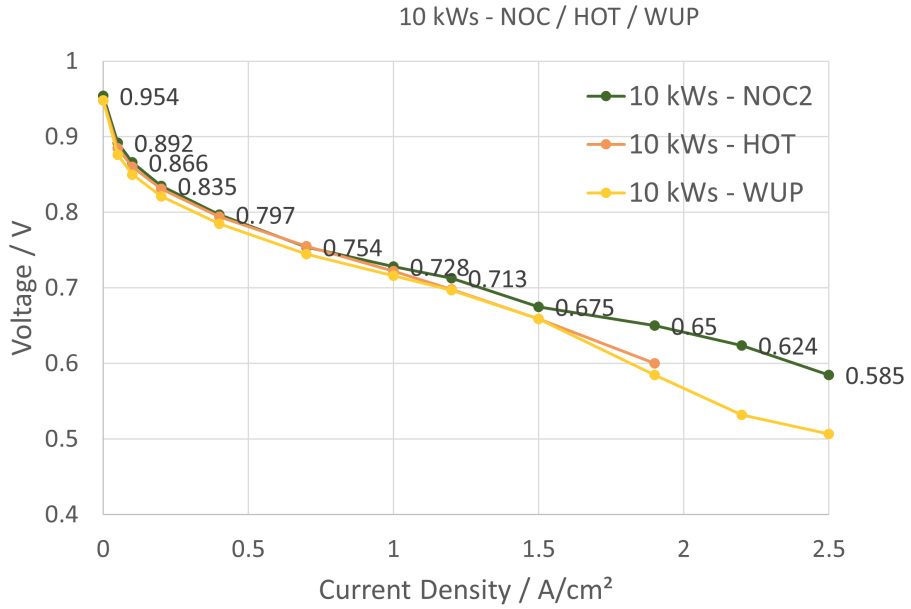


**Figure 4.7:** Polarization curves of the MEA produced from electrode dispersed to 10 kWs, tested in normal, hot and warm-up operating conditions.

The open circuit voltage is similar for all operating conditions, as expected. Because the losses at 0 A/cm$^2$ is attributed to hydrogen cross over should there not be any difference between operating conditions. At the kinetic point at 0.1 A/cm$^2$ the activation losses are dominant meaning that similar value between the different operating conditions implies that different conditions do not effect the utilization of catalyst. The mass transport losses seen for the HOT and WUP but not the NOC2 can be due the dry-up of the electrodes resulting in loss of accessible catalyst area.

The polarization curves for the MEAs produces from the electrode made with the ink dispersed to 50 kWs for normal, hot and warm-up operating conditions are presented in Fig. 4.8. Data points are shown for NOC2 and the open circuit voltage can be seen to be 0.935 V. The cell voltage at 0.1 A/cm$^2$ is 0.852 V and then decreases linearly to around 2.2 A/cm$^2$. Mass transport losses can be seen between 2.2 and 2.5 A/cm$^2$ with the final cell voltage is 0.572 V. The hot operating conditions also exhibit a polarization curve very similar to the NOC2 with an open circuit voltage of 0.931 V and a cell voltage of 0.853 V at 0.1 A/cm$^2$. The mass transport losses are greater for the HOT with the curve decreasing at 1.5 A/cm$^2$ and going down to 0.581 V at 1.9 A/cm$^2$. The warm up operating condition show a open circuit voltage of 0.929 V, a cell voltage of 0.844 V at 0.1 A/cm$^2$ and a final voltage of 0.504 V at 2.5 A/cm$^2$.

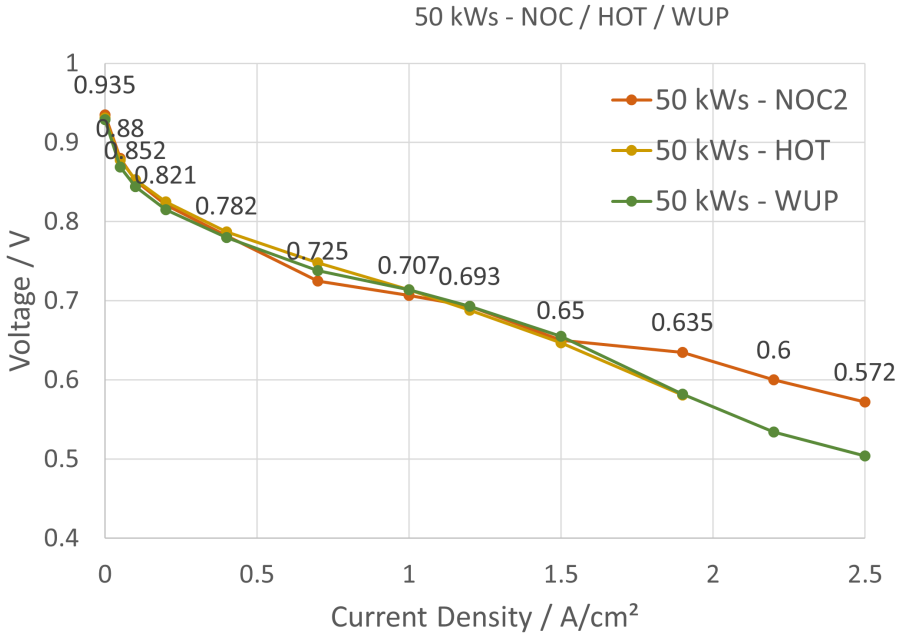


**Figure 4.8:** Polarization curves of the MEA produced from electrode dispersed to 50 kWs, tested in normal, hot and warm-up operating conditions.

The different operating conditions show very similar polarizing curves up until a current density of 1.5 A/cm$^2$. The HOT and WUP show the same mass transport loss and cell voltage of 0.581 and 0.582 V respectively at 1.9 A/cm$^2$.

Finally was the MEAs produced from the electrode made with the ink dispersed to 200 kWs tested. The polarization curve for the different conditions are presented in Fig. 4.9. NOC2 show an open circuit voltage of 0.968 V, a cell voltage of 0.867 V at 0.1 A/cm$^2$ and a linear decrease to 2.5 A/cm$^2$ with a final cell voltage of 0.57 V. The HOT curve show similarity to NOC2 until 1.5 A/cm$^2$ with an open circuit potential of 0.967 V, 0.867 V at 0.1 A/cm$^2$ and a mass transport losses resulting in a final cell voltage of 0.618 V at 1.9 A/cm$^2$. The WUP follows the trend of the other curves up until 1 A/cm$^2$, with an open circuit voltage of 0.963 V, a cell voltage of 0.852 V at 0.1 A/cm$^2$ but then show a significant decrease. The cell voltage at 2.5 A/cm$^2$ is 0.462 V.

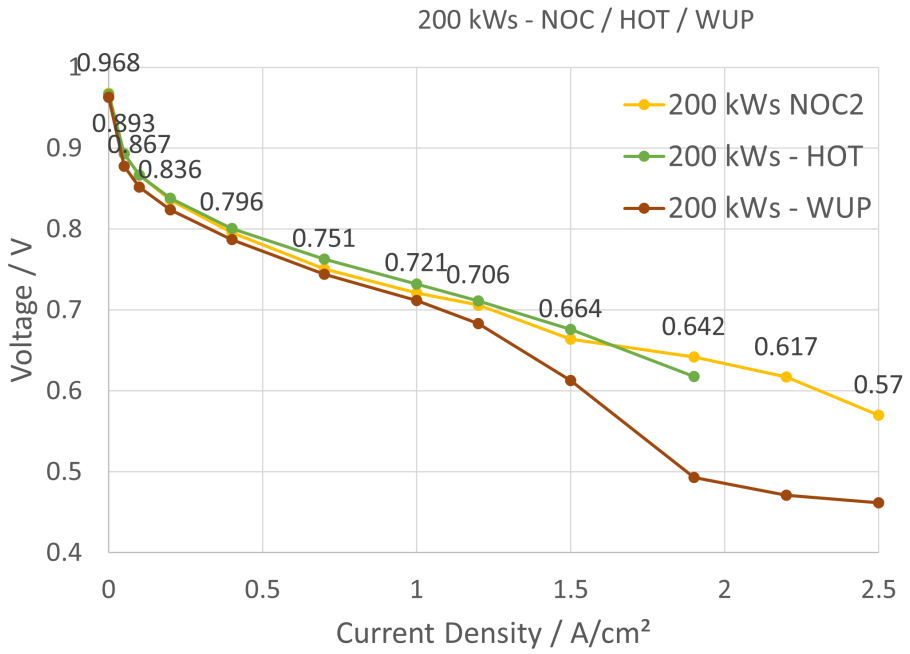


**Figure 4.9:** Polarization curves of the MEA produced from electrode dispersed to 200 kWs, tested in normal, hot and warm-up operating conditions.

The MEA perform very poorly after 1 A/cm$^2$ for the WUP which can the attributed to mostly mass transport losses. The relatively cold and wet conditions during WUP may result in flooding (41). It can be that high dispersion of the cathode resulted in a decrease in mesopores because of the break-up of agglomerates, resulting in mass transport limitations. The MEA can also have been damaged in some way that is not visible for the other tests as the WUP was the last test run the procedure. To avoid this uncertainty, several MEAs from the same cathode could have been tested.

The polarization curves for the three MEAs with differently dispersed electrodes tested under normal, hot and warm-up operating conditions are presented in Fig. 4.10 for comparison. For normal operating conditions it can be seen that curves for 10 and 200 kWs exhibit very similar values up until 1 A/cm$^2$, while the curves for 50 kWs display lower values. The MEAs exhibit significantly different open circuit potentials which is unexpected because all MEAs have the same membrane and preparation procedure which should result in same hydrogen cross over losses. Some changes might have occur during preparation that effects the open potential circuits. For the final voltage at 2.5 A/cm$^2$ the 10 kWs curve show the highest voltage of 0.585 V. Comparing these results to the sate of the art MEA produced in house, presented in Appendix B.5, it can be seen that the open circuit potential is lower for these curves but the voltage of all curves at 2.5 A/cm$^2$ are higher.

During hot operating conditions, the 200 kWs curve display the highest values and 50 kWs the lowest with 10 kWs in between, with all curves showing very similar shape. The open circuit potential is also here significantly different, which can attribute to the result at higher current densities. The 50 and 10 kWs curves for warm-up

operating conditions exhibit almost identical values while the 200 kWs curve show much worse performance. The results of the cathode from the ink dispersed to 50 kWs is unexpected as it was thought that it would perform better then the 10 kWs dispersed cathode, due to smaller agglomerates. Because of the differences in open circuit potential and otherwise small differences between the differently dispersed MEAs, no significant effect of dispersion can be concluded. The catalyst used for these test have a high activity so the effect of dispersion might not be significant at beginning of life. Replications of the tests and durability tests are needed for further investigation of dispersion energy on electrode performance.

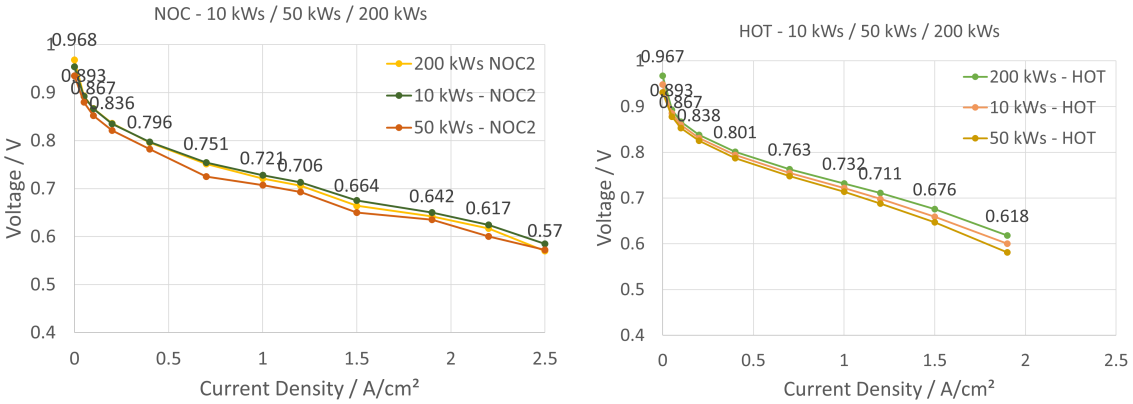


**(a)** Normal operating conditions **(b)** Hot operating conditions

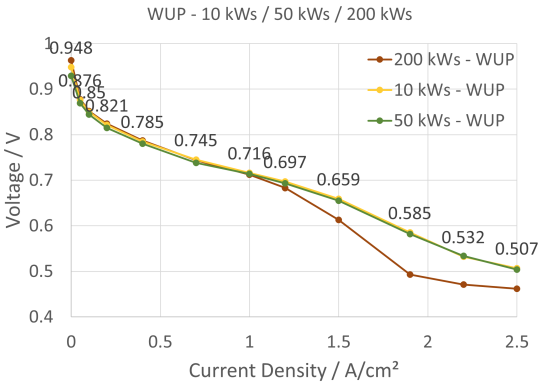


**(c)** Warm-up operating conditions

**Figure 4.10:** Polarization curves for MEAs produced with cathodes dispersed to 10, 50 and 200 kWs during normal, hot and warm-up operating conditions.

### 4.2.2 KB 3000 and SSC Ionomer

The rheology of an ink with KB 3000 and SSC ionomer is presented in Fig. 4.11. The ink show a very high viscosity for the undispersed sample that decrease after dispersion up to 10 kWs. The viscosity then increases again after dispersion up to 50 kWs. The viscous modulus is low for all samples with the ink dispersed to 10 kWs also here showing the lowest values.

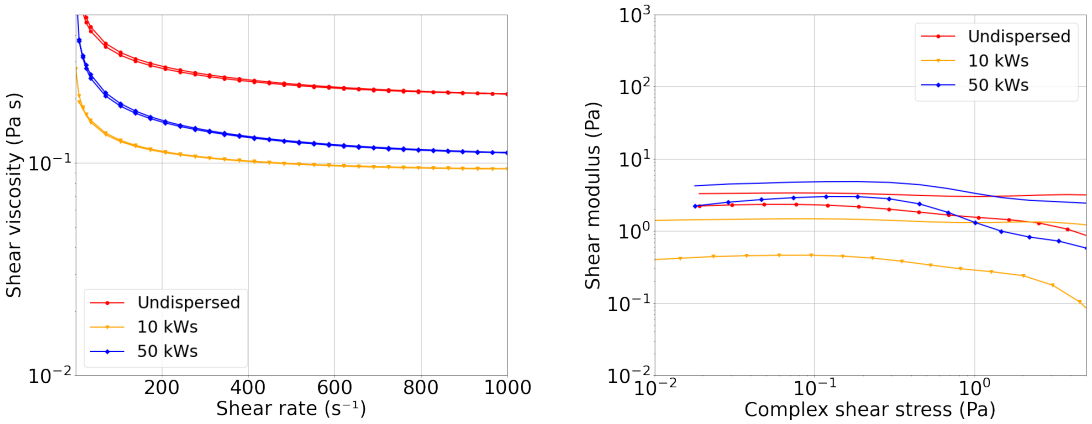


**(a)** Viscosity curves **(b)** Modulus curves

**Figure 4.11:** Rheological measurements of ink dispersion with KB 3000 and SSC ionomer undispersed and dispersed to 10, 50, 100 and 200 kWs.

The high viscosity of the undispersed sample can be attributed to the very agglomerates microstructure with high porosity. When the ink is dispersed, the agglomerates are partly broken up, decreasing the porosity and thus the viscosity. The increase in viscosity for the sample dispersed to 50 kWs could be attributed to a more well-dispersed microstructure with higher interactions between the ink components, resulting in a higher viscosity with a more shear-thinning behavior.

Micrographs of electrodes coated with 50 and 200 $\mu$m gap height for the ink left undispersed and dispersed to 10 and 50 kWs is presented in Appendix B.6. For the 50 $\mu$m coatings, there is a visible decrease in agglomerate size and the amount of agglomerates with increasing energy input. All coatings exhibit relatively smooth surfaces with no agglomerates of very large size. The 200 $\mu$m coating for the undispersed ink is also relatively smooth but with crack formation. The crack formation for the coating made from the 10 kWs dispersed ink is more severe with wider cracks and for the coating made with the ink dispersed to 50 kWs the cracks are even wider.

### 4.2.3 GCE Catalyst and SSC Ionomer

The rheological measurements for ink with GCE catalyst and SSC ionomer are presented in Fig. 4.12. The viscosity curve for the undispersed ink can be seen to drop below what visible in the graph and the ink dispersed to 50 kWs can also be seen to drop around a shear rate of 900 s $^{-1}$. This is because the samples splashed out of the rheometer during measurements and all results after these points are invalid. This did not happen to the inks dispersed to 100 and 200 kWs. The viscosity for the undispersed ink prior to splashing out is very low and it can be seen that the there is an increase in viscosity when comparing to the ink dispersed to 50 kWs before it also splashes out. The ink dispersed to 100 kWs show the highest viscosity and the ink dispersed to 200 kWs show the second highest viscosity. All inks show low shear modulus with the same trend as for the viscosity curves with with an

increase in modulus from undispersed to 100 kWs and then an decrease for the ink dispersed to 200 kWs. For all samples are the elastic component lower then the viscous component, hence showing undesirable modulus behavior for handling the ink.

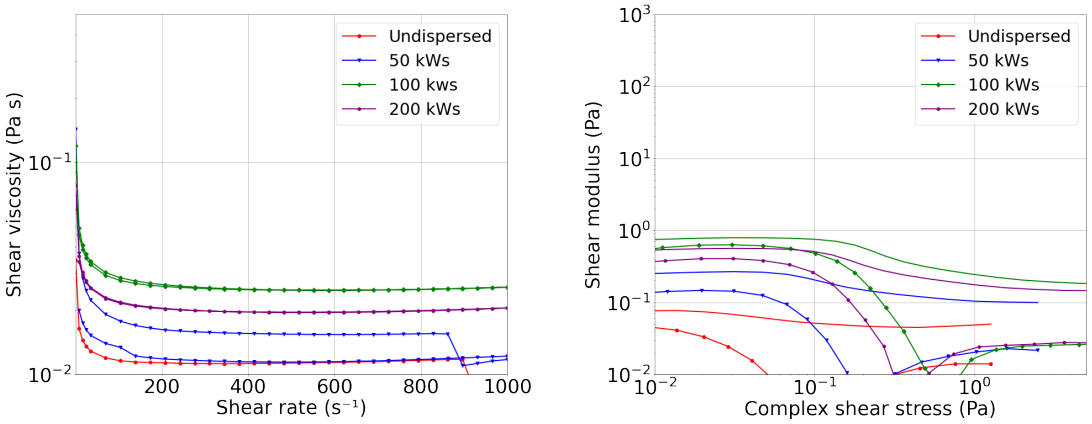


**(a)** Viscosity curves **(b)** Modulus curves

**Figure 4.12:** Rheological measurements of the ink with GCE catalyst and SSC ionomer undispersed and dispersed to 10, 50, 100 and 200 kWs.

Micrographs of electrodes made with the ink containing GCE catalyst and SSC ionomer and 50 $\mu$m gap height is presented in Fig. 4.13. Electrodes were made with the undispersed ink and inks dispersed to 10, 50, 100, 150 and 200 kWs. A trend can be seen from the images that the agglomerate decrease in size and abundance with increasing dispersion energy. The undispersed ink show the largest apparent agglomerates and the inks dispersed to 10 and 50 kWs both show the largest agglomerates found on the surface to be around 24 $\mu$m in diameter. It can be seen in the image though that the electrode from the ink dispersed to 50 kWs show fewer agglomerates in total. The ink dispersed to 100 kWs show even fewer agglomerates on the surface and the largest found measure about 16 $\mu$m in size. The electrodes made from the inks dispersed to 150 and 200 kWs show the largest agglomerates to be around 14 and 13 $\mu$m respectively. Despite the undesired rheological behavior, the electrodes seem to show good structures.

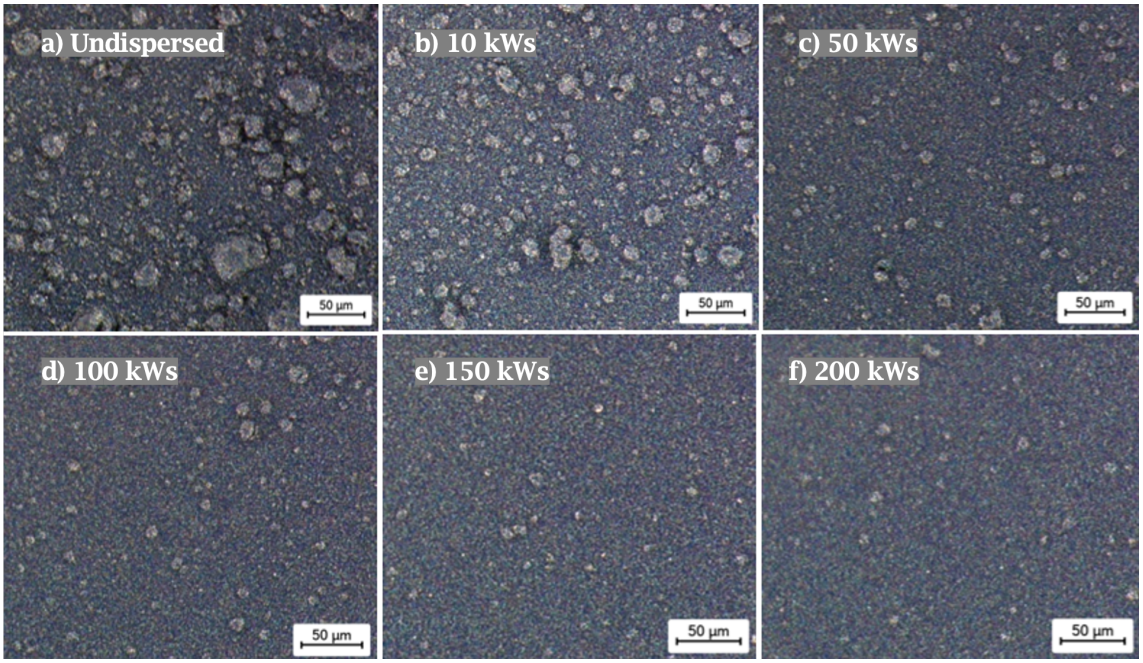


**Figure 4.13:** Micrographs with 500x magnification of 50 $\mu$m coatings from ink with GCE catalyst and SSC ionomer dispersed to 50, 10, 100, 150 and 200 kWs.

Micrographs of the coatings made with 200 $\mu$m gap height are presented in Appendix B.7. The agglomerate size and abundance can be seen to decrease from the undispersed coating to the 50 kWs dispersed one. The 100 kWs coating exhibit crack formation and apparent agglomerates can be seen. The 200 kWs dispersed coating display a few shallow cracks and much smaller agglomerates.

### 4.2.4 HCE Catalyst and LSC Ionomer

To further investigate the effect of ink components on the dispersion method and resulting electrodes, inks were made with a less temperature sensitive long side chain (LSC) ionomer. The rheological results for the ink made with HCE catalyst and LSC ionomer are presented in Fig. 4.14. The ink was analyzed when undispersed and dispersed to 50, 100, 150 and 200 kWs. All inks show a low viscosity at higher shear rates but very strong shear thinning behavior with high viscosity at low shear rates. The general viscosity decreases with increasing dispersion, except for the undispersed ink. The modulus curves show a desirable behavior for all ink with high modulus as well as higher elastic components than viscous components. The inks dispersed to 50 and 100 kWs show almost identical modulus curves with high elastic component that do not drop until after one Pa in shear stress. The ink dispersed to 200 kWs show the lowest modulus among the samples but the behavior of the curves still show good properties as the elastic component is higher than the viscous. The undispersed ink and the ink dispersed to 150 kWs show very similar values for both the elastic and viscous component but the elastic components can be seen to drop of faster for the undispersed ink.

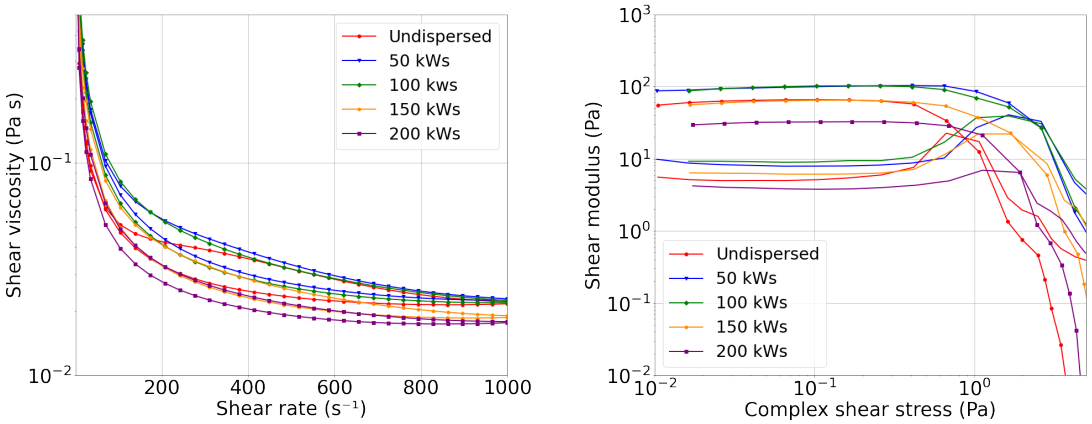


**(a)** Viscosity curves **(b)** Modulus curves

**Figure 4.14:** Rheological measurements of the ink with HCE catalyst and LSC ionomer for undispersed sample and dispersed to 50, 100 and 200 kWs.

When comparing the rheological properties of the ink with HCE catalyst and LSC ionomer with the ink containing HCE catalyst and SSC ionomer dispersed to the same energies, it is clear that the type of ionomer has a big effect on the rheological properties. The viscosity curves between the two inks are very different with the LSC ink showing much higher initial viscosity and a stronger shear-thinning behavior. The effect of dispersion on the viscosity is also not as strong for the LSC ink but with ink show a decrease in viscosity from the 100 to 200 kWs dispersed inks. The modulus curves for the LSC is better for all differently dispersed samples while the SSC ink only show nice modulus for the more highly dispersed inks. The ultrasonication energy input has hence different effects on the rheology depending on the ink components.

Four micrographs of 50 $\mu$m thick coatings for the ink dispersion with HCE catalyst and LSC ionomer are presented in Fig. 4.15. The panel show micrographs of samples that was left undispersed or dispersed up to 50, 100 and 200 kWs. The agglomerate size can clearly be seen to decrease from undispersed to 50 kWs ultrasonicated sample. The undispersed ink show several very large agglomerates with a diameter of up to 75 $\mu$m and many parts were the decal is not covered by ink. The coatings made with dispersed inks show a much more homogeneous structure where some agglomerates still are visible but the visible size and amount has decreased. The electrode made from the ink dispersed to 50 kWs show the largest visible agglomerate to be around 15 $\mu$m in size. The ink dispersed to 100 kWs exhibit a continued decrease in agglomerate size and abundance. It can be seen in the upper part of the coating that cracks of lengths around 40 $\mu$m have formed, visible by the back light shining through. The electrode of the ink dispersed to 200 kWs show even fewer agglomerates but there are still visible agglomerates of around 8 $\mu$m in size. The coating has less structure to the surface and no cracks have formed. It is clear from Figure 4.15 that the degree of dispersion increase with increasing total energy input.

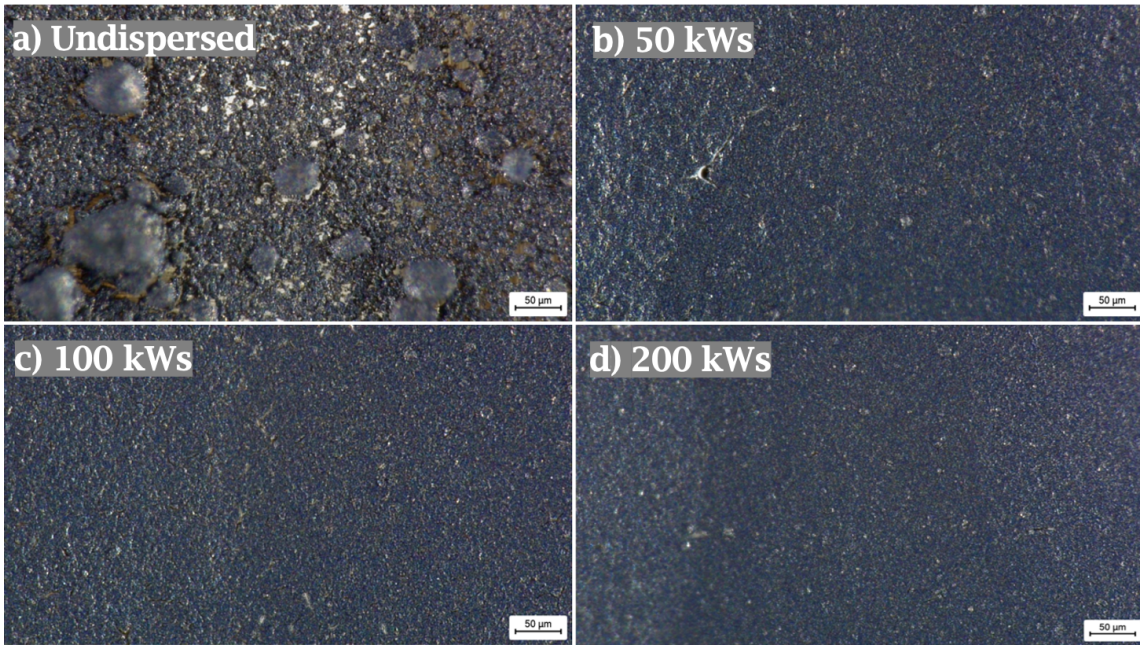


**Figure 4.15:** Micrographs with 500x magnification of 50 $\mu$m coatings from ink with HCE catalyst and LSC ionomer left undispersed and dispersed to 50, 100 and 200 kWs.

Comparing the micrographs to the findings for the ink containing HCE catalyst and SSC ionomer, the effects of ionomer on dispersion can be seen. The coatings from the undispersed ink both show agglomerates in the same size-range but the SSC ink do not show holes in the coating like the LSC ink. The dispersed coatings for the LSC ink show smaller agglomerates compared to the corresponding coatings for the SSC ink. Hence have the ionomer an effect on the break-up of agglomerates during ultrasonication.

Figure 4.16 presents the coatings made with 200 $\mu$m gap height of ink with HCE catalyst and LSC ionomer for the undispersed sample and the samples dispersed to 50, 100, and 200 kWs. The undispersed coating exhibit a very rough structure with large agglomerates and it is clear that the catalyst is very poorly dispersed into the ink solution before coating. The coating of the sample dispersed up to 50 kWs also show a cracked structure but the overall structure of the coating have changed and agglomerates have been dispersed resulting in a smoother surface of the coating. The dispersed coatings exhibit a tessellated structure with increasing tile size for increased energy input. The increase in tile size can be attributed to the highly dispersed inks being more resilient to stresses formed when the solvent evaporates resulting in fewer cracks compared to the 50 kWs dispersed ink. The inks are not totally resilient thought, resulting in fewer cracks that becomes wide as the tiles shrink from solvent evaporation.

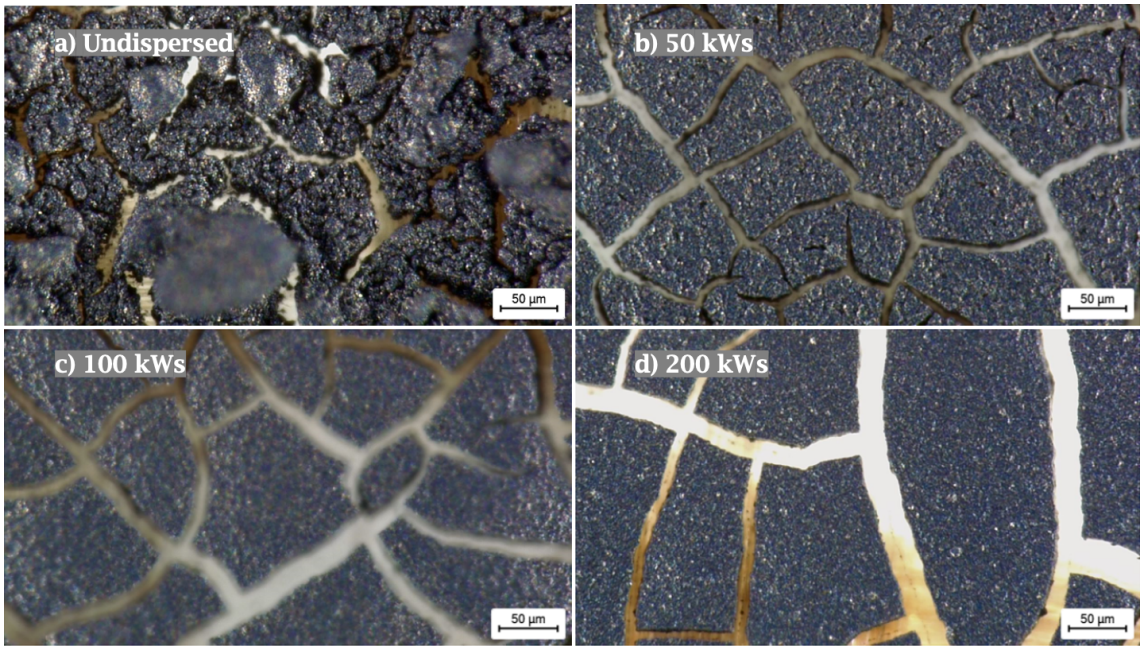


**Figure 4.16:** Micrographs with 500x magnification of 200 $\mu$m coating from the ink containing HCE catalyst and LSC ionomer left undispersed and dispersed to 50, 100 and 200 kWs.

### 4.2.5 HCK Catalyst and LSC Ionomer

To further investigate the effect of ink components on dispersion method, an ink with HCK catalyst and LSC ionomer was investigated. The rheological measurements for inks left undispersed and dispersed to 50, 100 and 200 kWs are presented in Fig. 4.17. The inks show a strong shear thinning behavior with low viscosity at relativity low shear rates. The ink dispersed to 200 kWs displays the lowest viscosity. The viscosity for low shear rates are higher for the ink dispersed to 100 kWs compared to the undispersed ink but decreases with increasing shear rate. The ink dispersed to 50 kWs show the highest viscosity among the samples. The undispersed ink and the ink dispersed to 200 kWs also show very low shear modulus while the inks dispersed to 50 and 100 kWs show slightly higher modulus. The elastic components for the inks dispersed to 50 and 100 kWs are higher than the viscous competent but the overall modulus is still low.

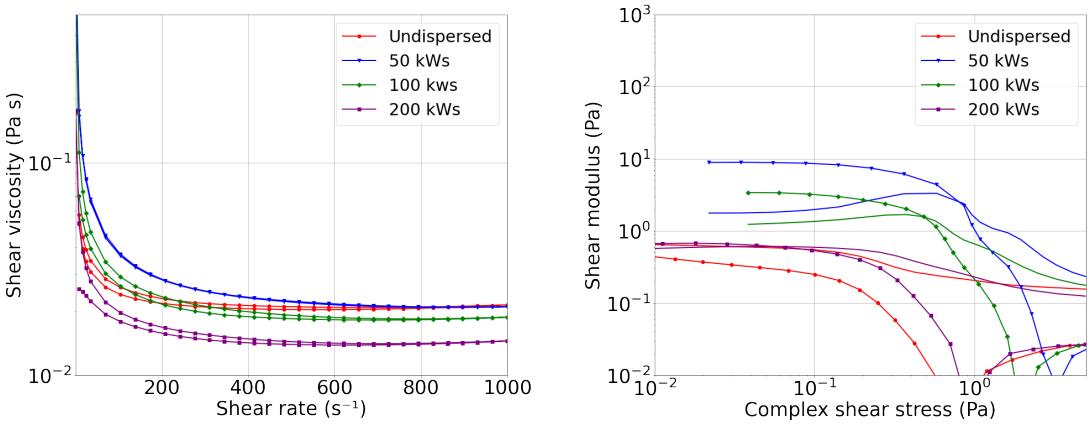


**(a)** Viscosity curves **(b)** Modulus curves

**Figure 4.17:** Rheological measurements of the ink with HCK catalyst and LSC ionomer undispersed and dispersed to 50, 100 and 200 kWs.

Micrographs of coatings made 50 and 200 $\mu$m gap height are presented in Appendix B.9 and B.10. The 50 $\mu$m coating of the ink dispersed to 50 kWs is not presented because the file got corrupted. The effect of dispersion is visible in the decrease in agglomerate size from 125 $\mu$m for the undispersed sample to 46 and 23 $\mu$m for the inks dispersed to 100 and 200 kWs respectively. Relatively large agglomerates are still apparent for the highly dispersed coatings, suggesting that the effect of ultrasonication on the microstructure of the ink i less compered to other ink with different components. The coatings made with a gap height of 200 $\mu$m also exhibit large agglomerates on the surface and small cracks. The coatings to not display the same tessellated structure as many previous samples did which can be attributed to the heterogeneous microstructure of the ink.

## 4.3 Effect of Ultrasonication Setup

To investigate the effect of increasing temperature and effects of mixing of the ink during ultrasonication, the flow cell setup was analysed. Ink dispersions was made by the same recipe but in a double batch, due to the larger volume of the flow cell, resulting in two times the volume of ink compared to experiments with ultrasonication in a vial.

### 4.3.1 HCE Catalyst and SSC Ionomer

An ink containing HCE catalyst and SSC ionomer was analyzed when undispersed and after ultrasonication to 50, 100 and 200 kWs in the flow cell with cooling water of 5°C. Fig. 4.18 show the rheological measurements for all the samples. The viscosity can be seen to increase with increasing sonication energy input at low to medium shear rates. A large change in viscosity can also be seen between increasing and decreasing shear rate for all samples with the more highly dispersed inks showing

the largest difference. The modulus curves for the samples show low modulus for the undispersed sample that increase with increasing dispersion energy input. The sample dispersed to 100 kWs show a high elastic modulus that do not decrease until around one Pa in shear stress. The ink dispersed to 200 kWs show an even higher elastic modulus at low complex shear stress but it soon decreases with increasing shear stress.

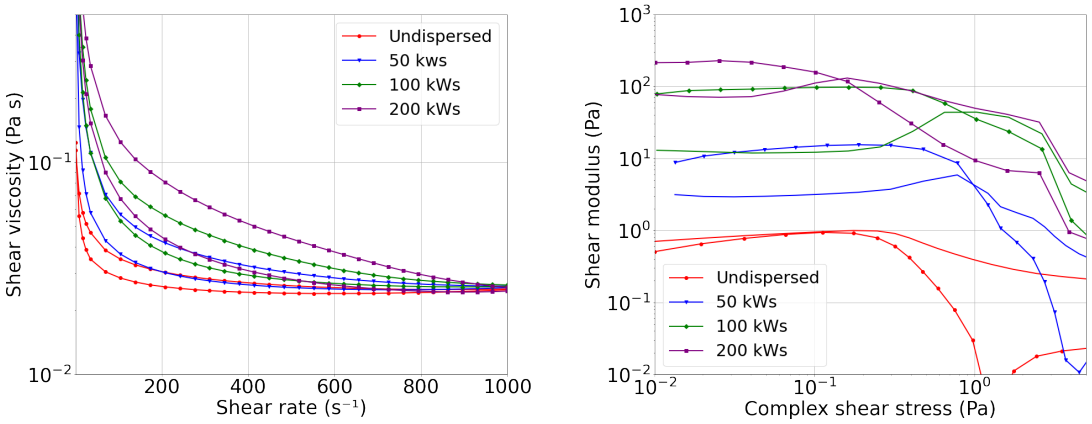


**(a)** Viscosity curves **(b)** Modulus curves

**Figure 4.18:** Rheological measurements of the ink containing HCE catalyst and SSC ionomer undispersed and dispersed to 50, 100 and 200 kWs with the flow cell setup.

When comparing these rheological results to the same ink recipe dispersed via ultrasonication in a vial showed in Fig. 4.5, it can be seen that the difference in viscosity for increasing and descending shear rates are only present for the lower dispersed inks. The ink dispersed in the flow cell do not show as strong shear thinning behavior but the viscosity for high shear rates are similar to the ink dispersed in a vial. The differences in rheological behavior suggests that the use of the flow cell during dispersion have an effect on the microstructure of the ink.

Micrographs of the coatings made with 50 $\mu$m gap height are presented in Fig. 4.19. All coatings exhibit relatively smooth surface structure and no large agglomerates. The agglomerate size and abundance can be seen to decrease with increasing energy input. The coating made from the inks dispersed to 50 and 100 kWs exhibit small cracks that appears to be shallow because the light from the back light do not shine trough.

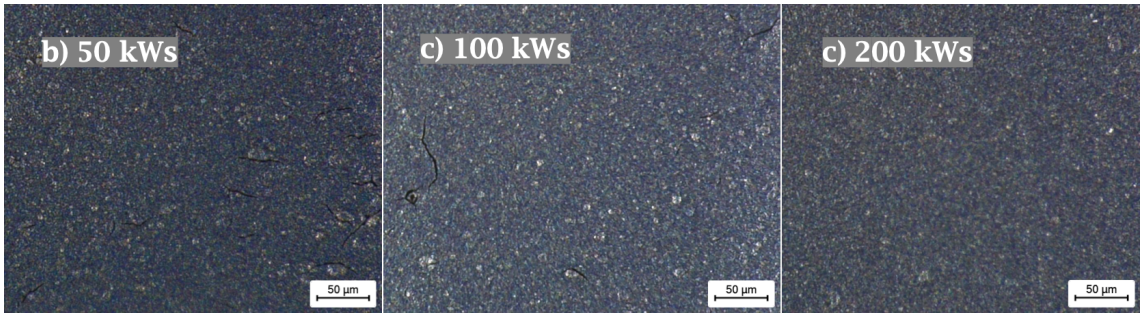


**Figure 4.19:** Micrographs with 500x magnification of 50 $\mu$m coatings from ink with HCE catalyst and SSC ionomer dispersed to 50, 100 and 200 kWs with the flow cell set-up.

It can be seen when comparing these coatings with the ones made from the ink dispersed in a vial that the coatings from the flow cell ink has more structure and small cracks of about 25 $\mu$m length. The coating from the ink dispersed in the vial show a smoother surface and no cracks, however agglomerates on the surface are abundant and can be seen to be up to 10 $\mu$m in diameter. Coatings with 200 $\mu$m gap height was only made for the 200 kWs dispersed ink because of limited ink supply. The micrograph is presented in Appendix B.8, and it can bee seen that the coating exhibit a similar tessellated structure as the inks dispersed in the vial. The tiles are smaller and exhibit a different shape suggesting a more agglomerated and less homogeneous structure of the ink compared to the ink dispersed in a vial.

If there would be overheating of the ink when dispersing in a vial with poor cooling, we would assume an increase in viscosity after dispersing for a relatively long time going from 10 kWs to 50 kWs. The viscosity measurements show no higher viscosity for the potentially overheated ink compared to the temperature controlled ink dispersed in the flow cell, meaning that the critical temperature where the ionomer start to gel was not reached. This is also indicated by the modulus curves as the two inks show very similar curves suggesting that the microstructure of the two inks are similar and have not been altered by the heat. The highest temperature measured for any ink was around 60 ° C and from other works in the lab it was found that the temperature at which the pure SSC ionomer start to gel was around 80°C. When investigating the 50 $\mu$m coatings of the two inks it is seen that the coating from the ink dispersed in the vial has less cracks but larger agglomerates on the surface compared to the coating from the ink dispersed in the flow cell. The 200 $\mu$m coating for the ink dispersed in the vial has cracked with larger tiles that are more separated while the coating from the flow cell ink has formed many more cracks and much smaller tiles.

### 4.3.2 GCE Catalyst and SSC Ionomer

Rheological measurements for an ink with GCE catalyst and SSC ionomer are presented in Fig. 4.20. A significant difference in viscosity and modulus can be seen between the undispersed and dispersed inks. The undispersed ink show a very low viscosity with low shear thinning behavior while the other inks show higher vis-

cosity and a shear thinning behavior. The ink dispersed to 100 kWs show that highest viscosity and the inks dispersed to 50 and 200 kWs show very similar viscosity curves. The 50 and 100 kWs dispersed inks show a high modulus while the 200 kWs dispersed ink show a initially high elastic component that rapidly decrease with increasing complex shear stress.

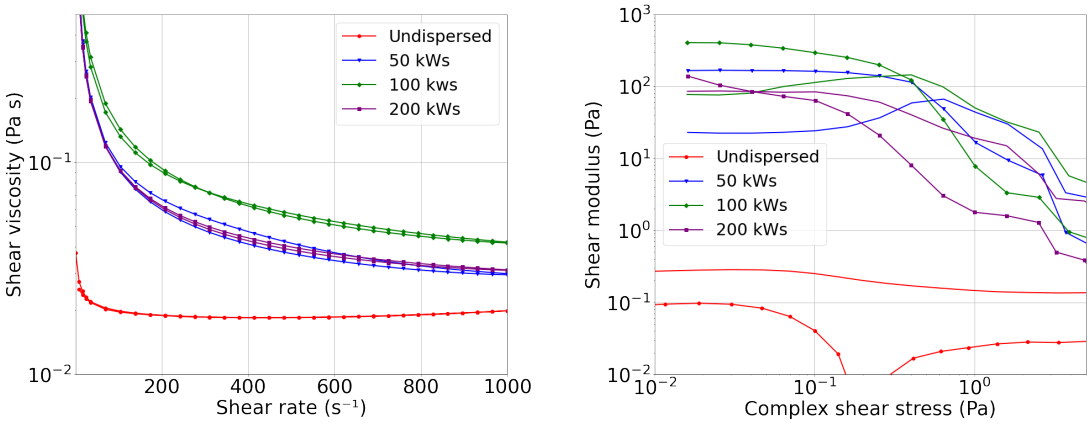


**(a)** Viscosity curves **(b)** Modulus curves

**Figure 4.20:** Rheological measurements of ink dispersion with GCE catalyst and SSC ionomer undispersed and dispersed to 50, 100 and 200 kWs with the flow cell setup.

Comparing the rheological behavior of this ink with the same recipe dispersed in a vial, a significant difference in both viscosity and modulus can be seen. The ink dispersed in the flow cell show much higher viscosity and a different shear thinning behavior. The modulus curves for the flow cell dispersed samples also show much higher values compared to ink dispersed in a vial where no samples had a shear modulus above one Pa in complex shear stress.

Micropgraphs of coatings made with 50 and 200 $\mu$m gap height for the ink dispersed to 200 kWs are presented in Fig. 4.21. Coating were not made for the other samples due to a limited amount of ink. The 50 $\mu$m thick coating exhibit small cracks and a rough surface while the 200 $\mu$m coating display more severe crack formation. The surface structure is very different compared to the same ink recipe dispersed in a vial. The coatings made from the ink dispersed in a vial showed much smoother surface structures.

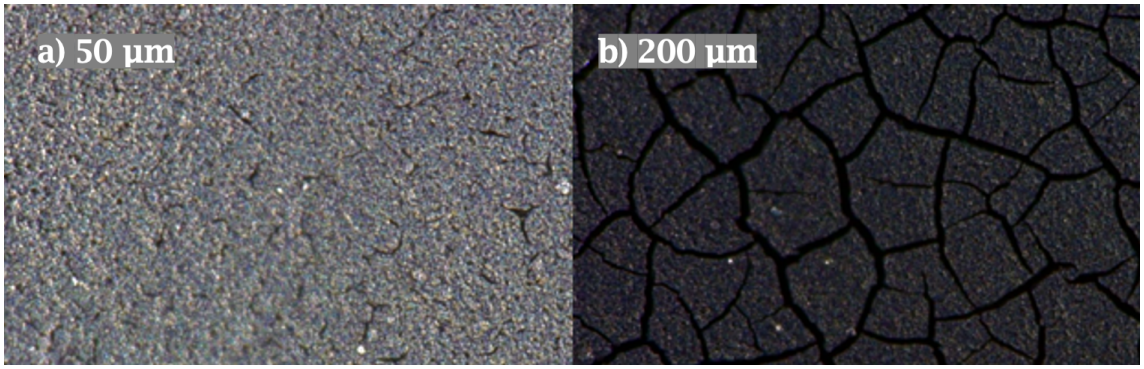


**Figure 4.21:** Micropgraphs with 500x magnification of coatings made with 50 and 200 $\mu$m gap height for ink containing GCE catalyst and SSC ionomer dispersed to 200 kWs.

### 4.3.3 HCE Catalyst and LSC Ionomer

Fig. 4.22 present the rheological measurements for ink with HCE catalyst and LSC ionomer when undispersed and dispersed to 50, 100 and 200 kWs. The ink dispersed to 50 kWs show the highest viscosity and the ink dispersed to 200 kWs the lowest. There is an increase in modulus from the undispersed ink to the one dispersed to 50 kWs but the modulus then decrease for the more highly dispersed inks. The ink dispersed to 200 kWs show a very low elastic component.

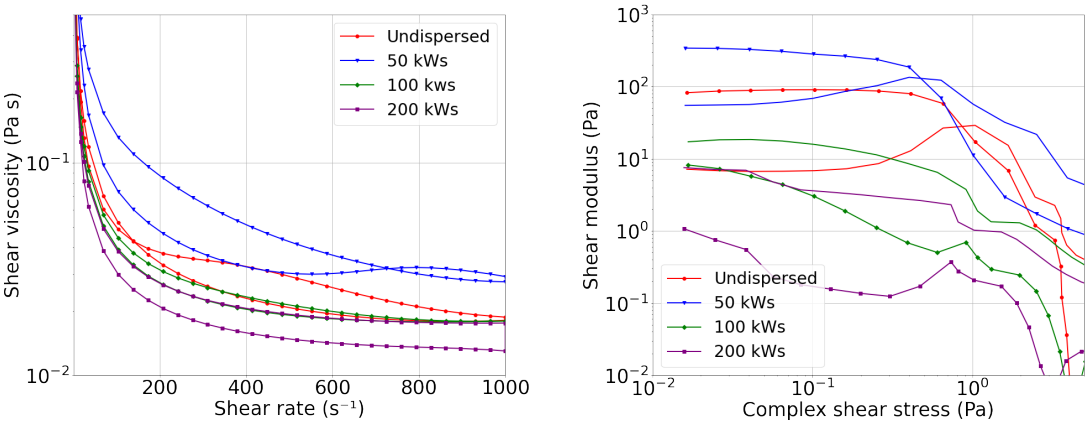


**(a)** Viscosity curves **(b)** Modulus curves

**Figure 4.22:** Rheological measurements of ink dispersion with HCE catalyst and SSC ionomer undispersed and dispersed to 50, 100 and 200 kWs with the flow cell setup.

Micrographs of coatings made with 50 and 200 $\mu$m gap height are presented in Appendix B.11. The coating made with a gap height of 50 $\mu$m gap height exhibit a rough surface structure and small cracks and the 200 $\mu$m thick a more severely cracked structure.

## 4.4 Effect of Bead-milling Dispersion Method

To investigate the effect of dispersion method on the rheological properties and agglomerate size of the catalyst ink, a different dispersion method was used. The inks were mixed by the same recipe as for ultrasonication experiments but in a plastic bottle with zirconium beads added to it. Bead-milling at 60 rpm for one day and three days respectively was applied.

### 4.4.1 HCE Catalyst and SSC Ionomer

Fig. 4.23 show the rheological measurements for ink with HCE catalyst and SSC ionomer after being dispersed by bead-milling for one day and three days respectively. The viscosity curves for the two samples are similar with the ink bead-milled for three days having a slightly higher viscosity. Both sample show a decrease in viscosity from increasing to decreasing shear rate and when compared to the ink sample that was dispersed with ultrasonication to 10 kWs, the viscosity curves are very similar. The modulus curves for the ink bead-milled for one day show low shear modulus values with the elastic component slightly higher than the viscous component. The ink bead-milled for three days show a lower shear modulus with an even lower elastic component.

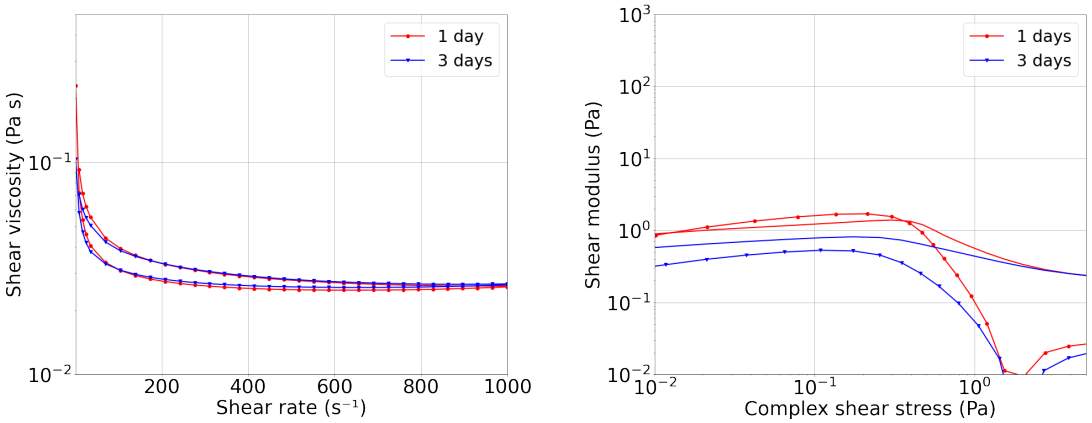


**(a)** Viscosity curves

**(b)** Modulus curves

**Figure 4.23:** Rheological measurements of ink dispersion with HCE catalyst and SSC ionomer dispersed by bead-milling for one and three days respectively.

Fig. 4.24 show micrographs of electrodes coated with 50 and 200 $\mu$m gap height for the two inks dispersed for one and three days. The 50 $\mu$m thick coating of the ink dispersed one day show few large agglomerates, with the largest one measuring 17.5 $\mu$m and a few cracks are visible by the back light. The corresponding 200 $\mu$m thick coating show severe crack formation. The 50 $\mu$m thick coating of the ink bead-milled for three days show a more homogeneous surface with very few visible agglomerates and the largest agglomerates found measured under 3 $\mu$m. The coating with 200 $\mu$m gap height show less severe crack formation with less wide cracks.

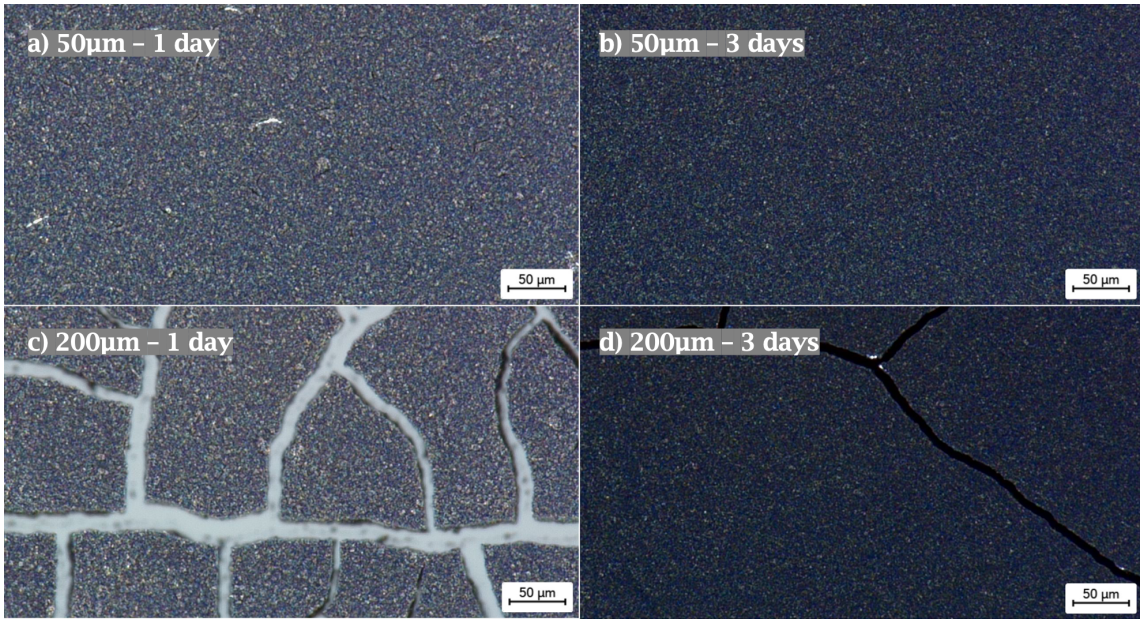


**Figure 4.24:** Micrographs with 500x magnification of 50 and 200 $\mu$m thick coatings from the ink with HCE catalyst and SSC ionomer dispersed by bead-milling for one and three days.

### 4.4.2 GCE Catalyst and SSC Ionomer

The rheological measurements of ink with GCE catalyst and SSC ionomer dispersed by bead-milling for one and three days are presented in Fig. 4.25. Both samples show low viscosity and low shear thinning behavior, with the ink dispersed for three days showing a slightly higher viscosity. The modulus curves also show low values and similarities between the two samples, with the ink dispersed for three days also here showing slightly higher values.

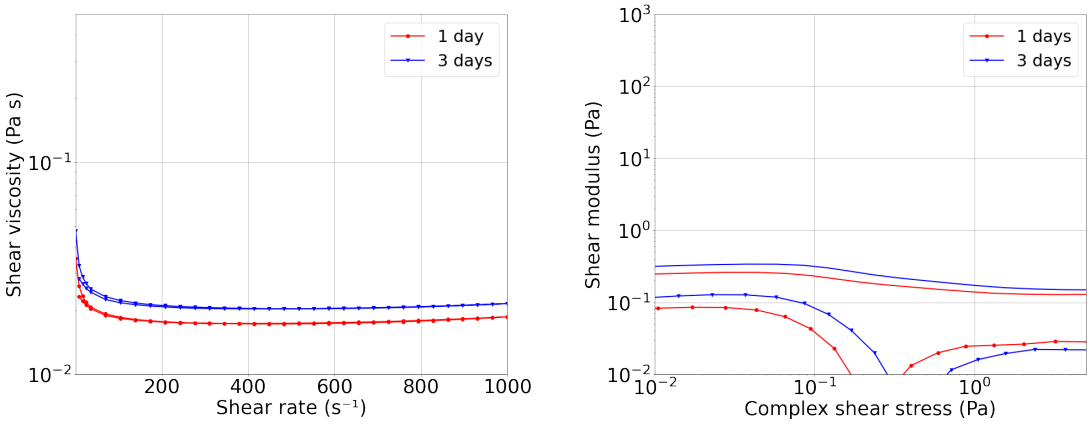


**(a)** Viscosity curves **(b)** Modulus curves

**Figure 4.25:** Rheological measurements of ink dispersion with GCE catalyst and SSC ionomer dispersed by bead-milling for one and three days respectively.

Micrographs of coating made with 50 and 200 $\mu$m gap height for both samples are presented in Fig. 4.26. The coatings made from the ink bead-milled for one day display smooth surfaces with some larger agglomerates visible. The ink dispersed for three days also show smooth coating with fewer and smaller agglomerates. All coatings exhibit less agglomerates then the coating made from the same ink recipe dispersed by ultrasonication. Comparing the coatings with 200 $\mu$m thickness with 200 kWs ultrasonicated ink coating with the same thickness, it can be seen that the bead-milled coatings less agglomerates and no cracks like the ultrasonicated coating.

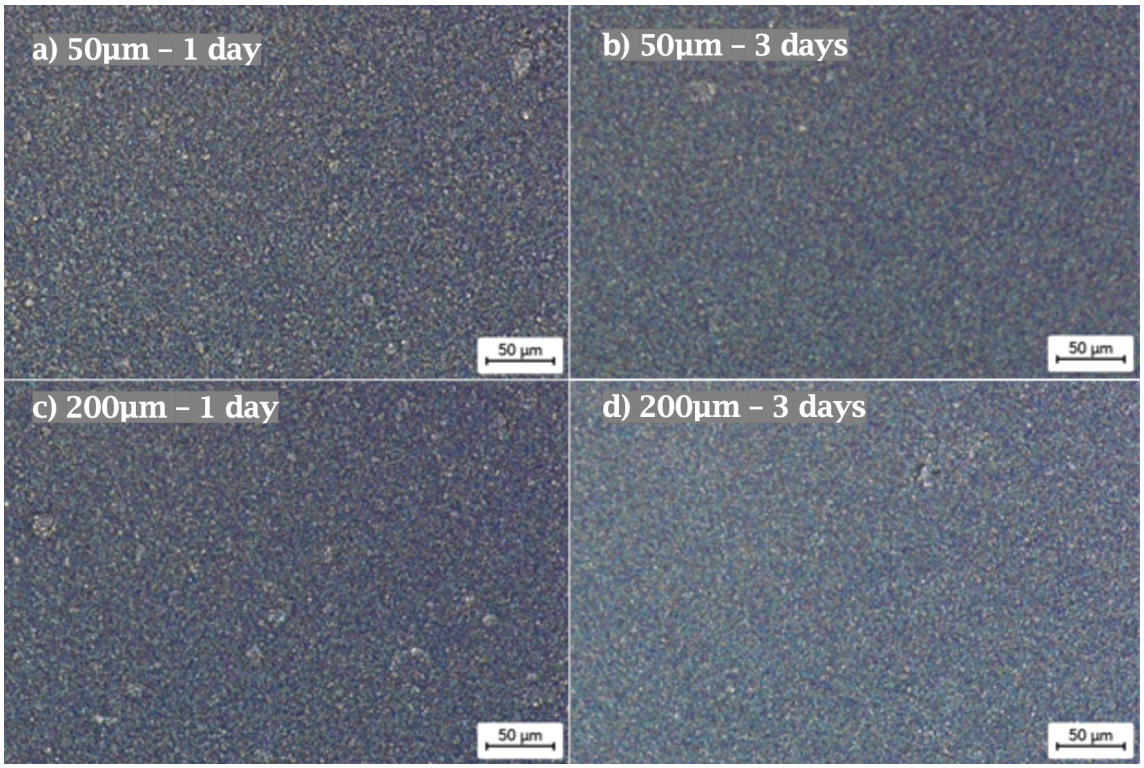


**Figure 4.26:** Micrographs with 500x magnification of coatings made with 50 and 200 $\mu$m gap height form ink with GCE catalyst and SSC ionomer dispersed by bead milling for one or three days.

### 4.4.3 HCK Catalyst and LSC Ionomer

The rheological measurements for the ink containing HCK catalyst and SSC ionomer dispersed by bead-milling for one and three days are presented in Fig. 4.27. The ink exhibit almost identical rheological behavior for the two dispersion times, with a strong shear thinning behavior, high viscosity and a relatively high modulus.

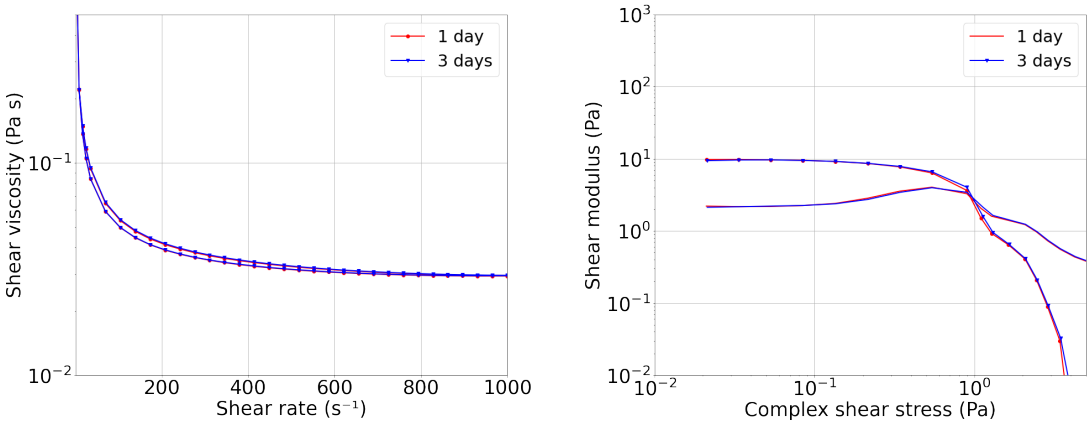


**(a)** Viscosity curves

**(b)** Modulus curves

**Figure 4.27:** Rheological measurements of ink dispersion with HCK catalyst and LSC ionomer dispersed by bead-milling for one and three days.

Comparing the rheological measurement to the same ink recipe dispersed by ultrasonication seen in Fig. 4.17, it can be seen that the viscosity is similar to the viscosity of the ink dispersed to 50 kWs via ultrasonication. The modulus curves are also very similar to that of the 50 kWs ultrasonicated sample.

Micropgraphs of the ink bead-milled for three days are presented in Appendix B.12. The coating made with 50 $\mu$m gap height do not display any large apparent agglomerates but exhibits a rough surface structure with many small cracks visible by the back light shining trough. The coating made with 200 $\mu$m gap height also display a rough surface structure and larger cracks. The coatings made with 50 $\mu$m gap height from the same ink recipe that had been dispersed with ultrasonication showed much smoother surface structures and fewer cracks. Comparing the 200 $\mu$m thick coating from the bead-milled ink with the 50 kWs ultrasonicated ink, the structures can be seen to be very similar.

# 5
# Conclusion

The objective of this thesis was to determine the effect of dispersion methodology on catalyst ink, and investigate the effect of catalyst ink materials, dispersion technique and parameters on the microstructure of the ink. It was found that increased vibrational amplitude during ultrasonication resulted in more well dispersed inks with electrodes displaying smaller and less abundant agglomerates. The vibrational amplitude was found to have an effect on the rheological behavior of the inks, suggesting it influences the ink microstructure during ultrasonication. The investigation of the effects from ultrasonic energy input showed that the ink components strongly influence the rheological behavior and resulting structure of the electrodes. It was found that increasing ultrasonic energy input significantly effects the rheological behavior of the inks and that high energy inputs can have both positive and negative effects on the rheology of inks depending on ink components. For the ink containing HCE catalyst and SSC ionomer, the optimum rheological behavior was found at an energy input of 100 kWs. The ink containing GCE catalyst and SSC also showed optimum rheological behavior at 100 kWs dispersion. An optimum energy input of 50 kWs was found for two inks containing HCE catalyst and LSC ionomer and HCK catalyst and LSC ionomer. It is hence concluded that no single dispersion procedure can be established for optimum dispersion of all ink recipes, and that the dispersion procedure needs to be tailored to the ink components.

The micrographs show that increasing energy input results in decreasing agglomerate size and abundance. Electrodes made with a gap height of 50 $\mu$m from the highest dispersed samples display smooth surface structures with few agglomerates only up to 10 $\mu$m in size for most ink recipes. It can hence be concluded that rheological measurements can only partly capture complex characteristics of the agglomerated structures and that highly dispersed ink with few and small agglomerates can show poorer rheological behavior compared to more agglomerated structures. The effect of ultrasonic energy input on the electrode performance was tested with in-situ testing for MEAs made from HCE catalyst and SSC ionomer containing inks dispersed to 10, 50 and 200 kWs. While no significant effect of dispersion energy could be concluded, the performance at high current densities exceeded that of the current state of the art in-house MEA. Temperature control and extensive mixing of the ink during ultrasonication was shown to strongly influence the rheological behavior and final electrode structure. A significant increase in viscosity and modulus was found for the ink containing HCE catalyst and SSC ionomer, with the electrodes exhibiting fewer agglomerates. The bead-milling dispersion method was found to give different rheological properties of the ink and more homogeneous electrodes.

With the results from this thesis, an optimization of the ink dispersion process was achieved, enabling the determination of dispersion design rules, e.g. regarding ultrasonic power and energy input.

# Bibliography


[1] Majlan EH, Rohendi D, Daud WRW, Husaini T, Haque MA. Electrode for proton exchange membrane fuel cells: A review. Renewable and Sustainable Energy Reviews. 2018;89:117–134. Available from: https://www.sciencedirect.com/science/article/pii/S1364032118300935. doi: https://doi.org/10.1016/j.rser.2018.03.007.

[2] Bapat S, Giehl C, Kohsakowski S, Peinecke V, Schäffler M, Segets D. On the state and stability of fuel cell catalyst inks. Advanced Powder Technology. 2021;32(10). Available from: https://www.sciencedirect.com/science/article/pii/S0921883121004040. doi: 10.1016/j.apt.2021.08.030.

[3] Ganesan A, Narayanasamy M. Ultra-low loading of platinum in proton exchange membrane-based fuel cells: a brief review. Materials for Renewable and Sustainable Energy. 2019;8(4). Available from: https://link.springer.com/article/10.1007/s40243-019-0156-x. doi: 10.1007/s40243-019-0156-x.

[4] Barbir F. Chapter One - Introduction. In: Barbir F, editor. PEM Fuel Cells. 2nd ed. Boston: Academic Press; 2013. p. 1–16. Available from: https://www.sciencedirect.com/science/article/pii/B9780123877109000011. doi: https://doi.org/10.1016/B978-0-12-387710-9.00001-1.

[5] Guo S, Zhang S, Sun S. Tuning nanoparticle catalysis for the oxygen reduction reaction. Angewandte Chemie - International Edition. 2013;52(33). Available from: https://onlinelibrary.wiley.com/doi/full/10.1002/anie.201207186. doi: 10.1002/anie.201207186.

[6] Eikerling M, Kornyshev AA, Kucernak AR. Water in polymer electrolyte fuel cells: Friend or foe? Physics Today. 2006;59(10). Available from: https://pubs.aip.org/physicstoday/article/59/10/38/412628/Water-in-polymer-electrolyte-fuel-cells-Friend-or. doi: 10.1063/1.2387087.

[7] Yuan XZ, Wang H. PEM Fuel Cell Fundamentals. Zhang J, editor. London: Springer London; 2008. Available from: https://link.springer.com/chapter/10.1007/978-1-84800-936-3_1. doi: 10.1007/978-1-84800-936-3_1.

[8] Song C, Zhang J. Electrocatalytic Oxygen Reduction Reaction. In: Zhang J, editor. PEM Fuel Cell Electrocatalysts and Catalyst Layers: Fundamentals and Applications. London: Springer London; 2008. p. 89–

134. Available from: https://link.springer.com/chapter/10.1007/978-1-84800-936-3_2. doi: 10.1007/978-1-84800-936-3_2.

[9] Barbir F. Chapter Three - Fuel Cell Electrochemistry. In: Barbir F, editor. PEM Fuel Cells. 2nd ed. Boston: Academic Press; 2013. p. 33–72. Available from: https://www.sciencedirect.com/science/article/pii/B9780123877109000035. doi: https://doi.org/10.1016/B978-0-12-387710-9.00003-5.

[10] Williams MV, Kunz HR, Fenton JM. Analysis of Polarization Curves to Evaluate Polarization Sources in Hydrogen/Air PEM Fuel Cells. Journal of The Electrochemical Society. 2005;152(3). Available from: https://iopscience.iop.org/article/10.1149/1.1860034/meta. doi: 10.1149/1.1860034.

[11] Hirschenhofer JH, Stauffer DB, Engleman RR. Fuel Cell Handbook. Sixth ed. DIANE Publishing; 1994.

[12] Barbir F. Chapter Four - Main Cell Components, Material Properties, and Processes. In: Barbir F, editor. PEM Fuel Cells. 2nd ed. Boston: Academic Press; 2013. p. 73–117. Available from: https://www.sciencedirect.com/science/article/pii/B9780123877109000047. doi: https://doi.org/10.1016/B978-0-12-387710-9.00004-7.

[13] Malek K, Eikerling M, Wang Q, Navessin T, Liu Z. Self-organization in catalyst layers of polymer electrolyte fuel cells. Journal of Physical Chemistry C. 2007;111(36). Available from: https://pubs.acs.org/doi/abs/10.1021/jp072692k. doi: 10.1021/jp072692k.

[14] Antolini E. Structural parameters of supported fuel cell catalysts: The effect of particle size, inter-particle distance and metal loading on catalytic activity and fuel cell performance. Applied Catalysis B: Environmental. 2016;181. Available from: https://www.sciencedirect.com/science/article/pii/S0926337315300801. doi: 10.1016/j.apcatb.2015.08.007.

[15] Litster S, McLean G. PEM fuel cell electrodes. Journal of Power Sources. 2004;130(1-2). Available from: https://www.sciencedirect.com/science/article/pii/S0378775304000631. doi: 10.1016/j.jpowsour.2003.12.055.

[16] Zhang S, Yuan XZ, Hin JNC, Wang H, Friedrich KA, Schulze M. A review of platinum-based catalyst layer degradation in proton exchange membrane fuel cells. Journal of Power Sources. 2009;194(2). Available from: https://www.sciencedirect.com/science/article/pii/S037877530901146X. doi: 10.1016/j.jpowsour.2009.06.073.

[17] Feng Y, Alonso-Vante N. Nonprecious metal catalysts for the molecular oxygen-reduction reaction. Physica Status Solidi (B) Basic Research. 2008;245(9). doi: 10.1002/pssb.200879537.

[18] Jung N, Chung DY, Ryu J, Yoo SJ, Sung YE. Pt-based nanoarchitecture and catalyst design for fuel cell applications. Nano Today. 2014 8;9(4):433–

456. Available from: https://www.sciencedirect.com/science/article/pii/S1748013214000863. doi: 10.1016/j.nantod.2014.06.006.

[19] Shao Y, Liu J, Wang Y, Lin Y. Novel catalyst support materials for PEM fuel cells: Current status and future prospects. Journal of Materials Chemistry. 2009;19(1). Available from: https://pubs.rsc.org/en/content/articlehtml/2009/jm/b808370c. doi: 10.1039/b808370c.

[20] Teranishi K, Kawata K, Tsushima S, Hirai S. Degradation mechanism of PEMFC under open circuit operation. Electrochemical and Solid-State Letters. 2006;9(10). Available from: https://iopscience.iop.org/article/10.1149/1.2266163/meta. doi: 10.1149/1.2266163.

[21] Yasuda K, Taniguchi A, Akita T, Ioroi T, Siroma Z. Platinum dissolution and deposition in the polymer electrolyte membrane of a PEM fuel cell as studied by potential cycling. Physical Chemistry Chemical Physics. 2006;8(6). Available from: https://pubs.rsc.org/en/content/articlehtml/2006/cp/b514342j. doi: 10.1039/b514342j.

[22] Yang Z, Ball S, Condit D, Gummalla M. Systematic Study on the Impact of Pt Particle Size and Operating Conditions on PEMFC Cathode Catalyst Durability. Journal of The Electrochemical Society. 2011;158(11). Available from: https://iopscience.iop.org/article/10.1149/2.081111jes/meta. doi: 10.1149/2.081111jes.

[23] Eikerling MH, Malek K, Wang Q. Catalyst Layer Modeling: Structure, Properties and Performance. In: Zhang J, editor. PEM Fuel Cell Electrocatalysts and Catalyst Layers: Fundamentals and Applications. London: Springer London; 2008. p. 381–446. Available from: https://doi.org/10.1007/978-1-84800-936-3_8. doi: 10.1007/978-1-84800-936-3_8.

[24] Shen PK. PEM Fuel Cell Catalyst Layers and MEAs. In: Zhang J, editor. PEM Fuel Cell Electrocatalysts and Catalyst Layers: Fundamentals and Applications. London: Springer London; 2008. p. 355–380. Available from: https://doi.org/10.1007/978-1-84800-936-3_7. doi: 10.1007/978-1-84800-936-3_7.

[25] Wang M, Park JH, Kabir S, Neyerlin KC, Kariuki NN, Lv H, et al. Impact of Catalyst Ink Dispersing Methodology on Fuel Cell Performance Using in-Situ X-ray Scattering. ACS Applied Energy Materials. 2019;2(9). Available from: https://pubs.acs.org/doi/abs/10.1021/acsaem.9b01037. doi: 10.1021/acsaem.9b01037.

[26] Du S, Li W, Wu H, Abel Chuang PY, Pan M, Sui PC. Effects of ionomer and dispersion methods on rheological behavior of proton exchange membrane fuel cell catalyst layer ink. International Journal of Hydrogen Energy. 2020;45(53). Available from: https://www.sciencedirect.com/science/article/pii/S0360319920329165. doi: 10.1016/j.ijhydene.2020.07.241.

[27] Gedanken A. Sonochemistry and its application to nanochemistry. Cur-

rent Science. 2003;85(12). Available from: https://www.jstor.org/stable/24109977.

[28] Ultrasonic Dispersion of Nanomaterials (Nanoparticles) [Internet]; 2023. Available from: https://www.hielscher.com/nano_01.htm.

[29] Pollet BG. Let's Not Ignore the Ultrasonic Effects on the Preparation of Fuel Cell Materials. Electrocatalysis. 2014;5(4). Available from: https://link.springer.com/article/10.1007/s12678-014-0211-4. doi: 10.1007/s12678-014-0211-4.

[30] Pollet BG, Goh JTE. The importance of ultrasonic parameters in the preparation of fuel cell catalyst inks. Electrochimica Acta. 2014;128. Available from: https://www.sciencedirect.com/science/article/pii/S0013468613019658. doi: 10.1016/j.electacta.2013.09.160.

[31] Shinozaki K, Zack JW, Richards RM, Pivovar BS, Kocha SS. Oxygen Reduction Reaction Measurements on Platinum Electrocatalysts Utilizing Rotating Disk Electrode Technique. Journal of The Electrochemical Society. 2015;162(10). Available from: https://iopscience.iop.org/article/10.1149/2.1071509jes/meta. doi: 10.1149/2.1071509jes.

[32] Sharma S, Pollet BG. Support materials for PEMFC and DMFC electrocatalysts - A review. Journal of Power Sources. 2012;208. Available from: https://www.sciencedirect.com/science/article/pii/S0378775312003126. doi: 10.1016/j.jpowsour.2012.02.011.

[33] Liu H, Ney L, Zamel N, Li X. Effect of Catalyst Ink and Formation Process on the Multiscale Structure of Catalyst Layers in PEM Fuel Cells. Applied Sciences (Switzerland). 2022;12(8). Available from: https://www.mdpi.com/2076-3417/12/8/3776. doi: 10.3390/app12083776.

[34] O'Kane M. Solution Coating Methods: A Comparison;. Available from: https://www.ossila.com/pages/solution-processing-techniques-comparison.

[35] Harsha A, Ebenezer D, Siddhardha S, Alkesh A, Mal N. Studies on structure property relations of efficient decal substrates for industrial grade membrane electrode assembly development in pemfc. Scientific Reports. 2018;8(1). Available from: https://www.nature.com/articles/s41598-018-30215-0. doi: 10.1038/s41598-018-30215-0.

[36] Goodwin JW, Hughes RW. Rheology for Chemists. 2nd ed. Royal Society of Chemistry; 2008. doi: 10.1039/9781847558046.

[37] Khandavalli S, Park JH, Kariuki NN, Myers DJ, Stickel JJ, Hurst K, et al. Rheological Investigation on the Microstructure of Fuel Cell Catalyst Inks. ACS Applied Materials and Interfaces. 2018;10(50). Available from: https://pubs.acs.org/doi/abs/10.1021/acsami.8b15039. doi: 10.1021/acsami.8b15039.

[38] Basics of rheology [Internet];. Available from: https://wiki.anton-paar.com/en/basics-of-rheology/#c18437.

[39] Holgate JH, Webb J. Caballero B, editor. MICROSCOPY | Light Microscopy and Histochemical Methods. Elsevier; 2003. Available from: https://www.sciencedirect.com/science/article/pii/B012227055X007781. doi: 10.1016/b0-12-227055-x/00778-1.

[40] Rajalakshmi N, Dhathathreyan KS. Catalyst layer in PEMFC electrodes-Fabrication, characterisation and analysis. Chemical Engineering Journal. 2007;129(1-3). Available from: https://www.sciencedirect.com/science/article/pii/S1385894706004633. doi: 10.1016/j.cej.2006.10.035.

[41] Moore M, Wardlaw P, Dobson P, Boisvert JJ, Putz A, Spiteri RJ, et al. Understanding the Effect of Kinetic and Mass Transport Processes in Cathode Agglomerates. Journal of The Electrochemical Society. 2014;161(8). Available from: https://iopscience.iop.org/article/10.1149/2.010408jes/meta. doi: 10.1149/2.010408jes.

# A

# Appendix 1

## Ink Sample Overview

## A.1 Vibrational Amplitude Investigation

| Catalyst/ Support | Ionomer | Dispersion | Amplitude | Energy [kWs] |
|---|---|---|---|---|
| HCE | SSC | Ultrasonication | 20% | 10 & 50 |
| HCE | SSC | Ultrasonication | 50% | 10 & 50 |
| HCK | SSC | Ultrasonication | 20% | 10 & 50 |
| HCK | SSC | Ultrasonication | 50% | 10 & 50 |
| KB 3000 | SSC | Ultrasonication | 20% | 10 & 50 |
| KB 3000 | SSC | Ulrasonication | 50% | 10 & 50 |

## A.2 Ultrasonic Energy Input Investigation

| Catalyst/ Support | Ionomer | Dispersion | Amplitude | Energy [kWs] |
|---|---|---|---|---|
| HCE | SSC | Ultrasonication | 50% | 10, 50, 100 & 200 |
| KB 3000 | SSC | Ultrasonication | 50% | 10 & 50 |
| GCE | SSC | Ultrasonication | 50% | 50, 100 & 200 |
| HCE | LSC | Ultrasonication | 50% | 50, 100, 150 & 200 |
| HCK | LSC | Ultrasonication | 50% | 50, 100 & 200 |

## A.3 Ultrasonic Set-up Investigation

| Catalyst/ Support | Ionomer | Dispersion | Amplitude | Energy [kWs] |
|---|---|---|---|---|
| HCE | SSC | Ultrasonication Flow Cell | 50% | 50, 100 & 200 |
| GCE | SSC | Ultrasonication Flow Cell | 50% | 50, 100 & 200 |
| HCE | LSC | Ultrasonication Flow Cell | 50% | 50, 100 & 200 |

## A.4 Bead-milling Investigation

| Catalyst/ Support | Ionomer | Dispersion | Time |
|---|---|---|---|
| HCE | SSC | Bead-milling | 1 & 3 days |
| GCE | SSC | Bead-milling | 1 & 3 days |
| HCK | LSC | Bead-milling | 1 & 3 days |

# B

# Appendix 2

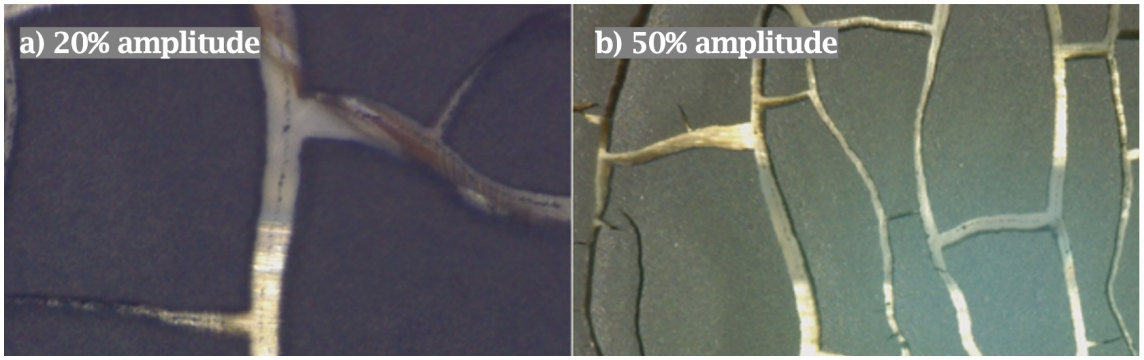


**Figure B.1:** Micrographs of coating made with 200 $\mu$m gap height from the ink with HCE catalyst and SSC ionomer dispersed with 20% and 50% amplitude. The micrograph to the left is taken with 500x magnification and the one to the right with 200x magnification.

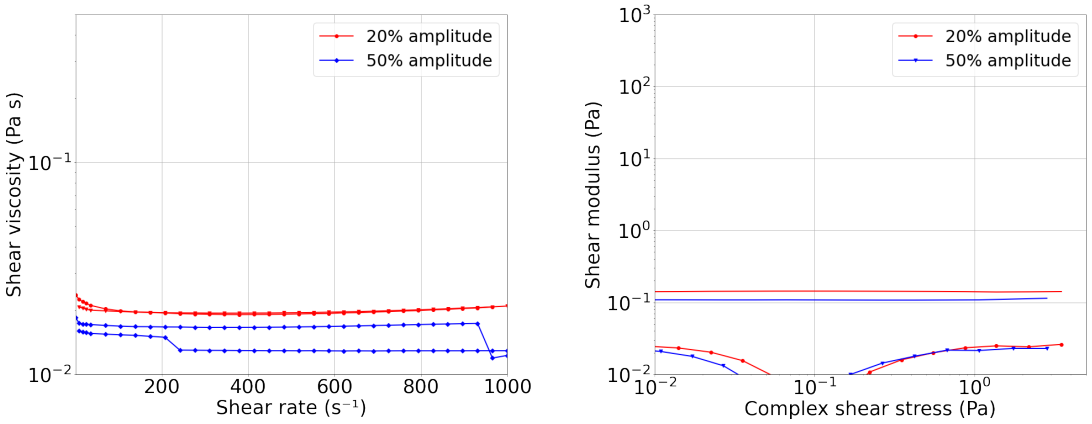


**(a)** Viscosity curves **(b)** Modulus curves

**Figure B.2:** Rheological measurements of the ink with HCK and SSC ionomer dispersed to 50 kWs with vibrational amplitude of 20% and 50%.

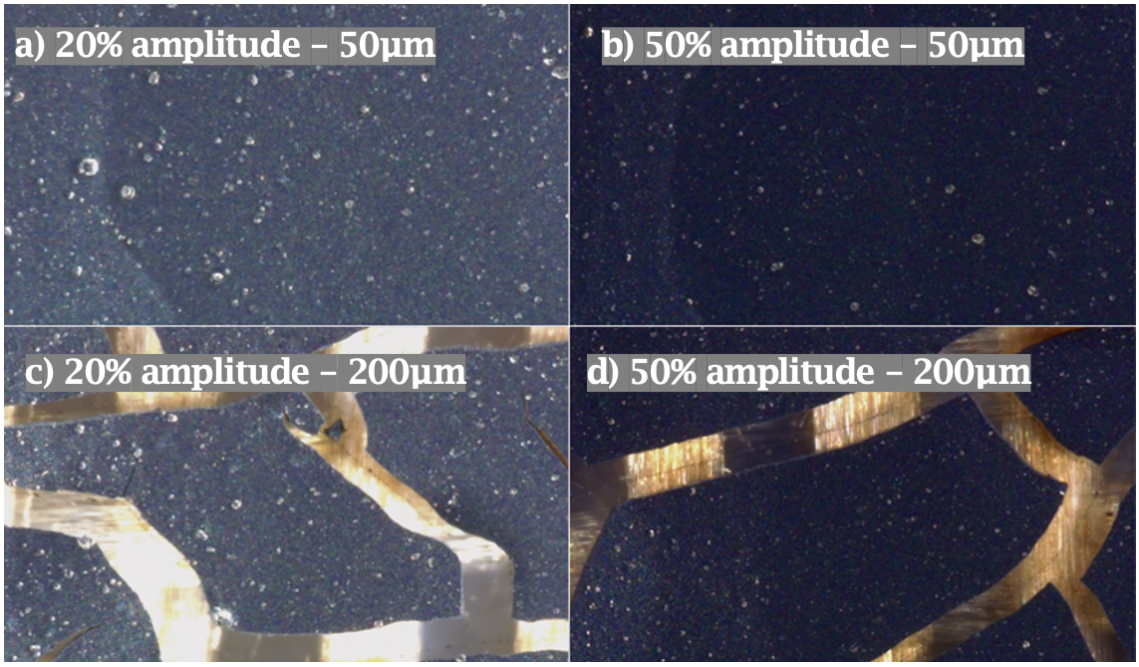


**Figure B.3:** Micrographs with 200x magnification of 50 $\mu$m and 200 $\mu$m thick coatings from ink with KB 300 and SSC ionomer dispersed with either 20% or 50% vibrational amplitude.

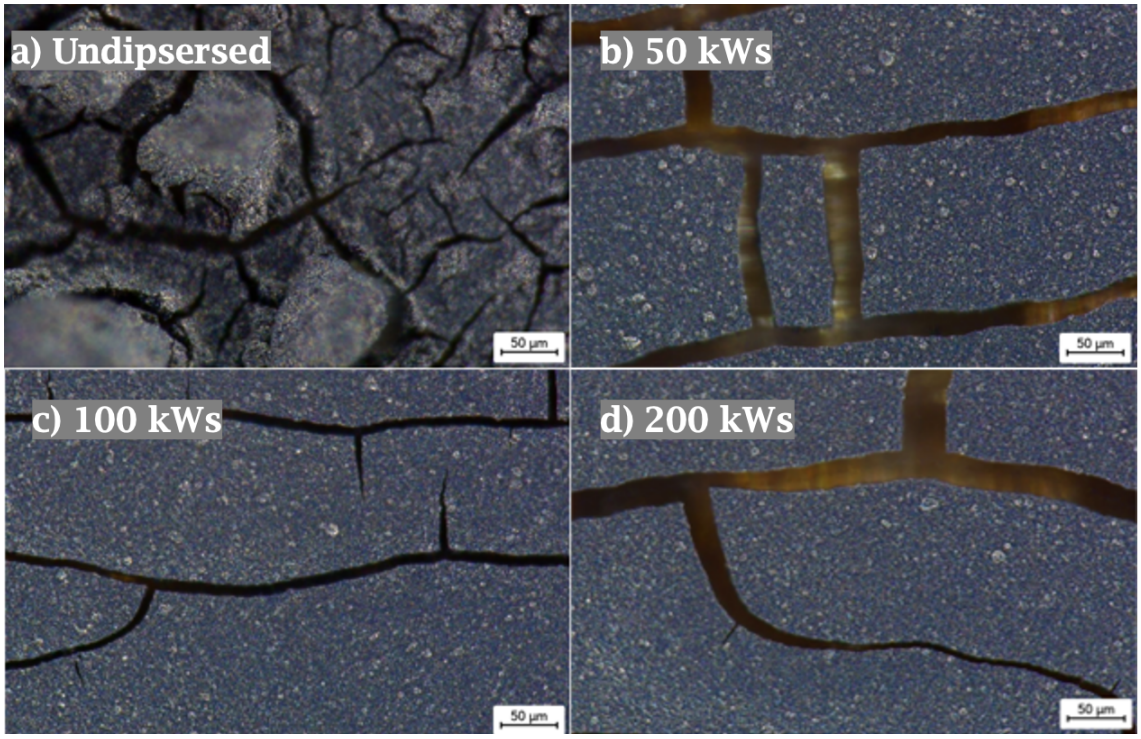


**Figure B.4:** Micrographs with 500x magnification of electrodes made with 200 $\mu$m gap height from ink with HCE catalyst and SSC ionomer left undispersed and dispersed to 50, 100 and 200 kWs.

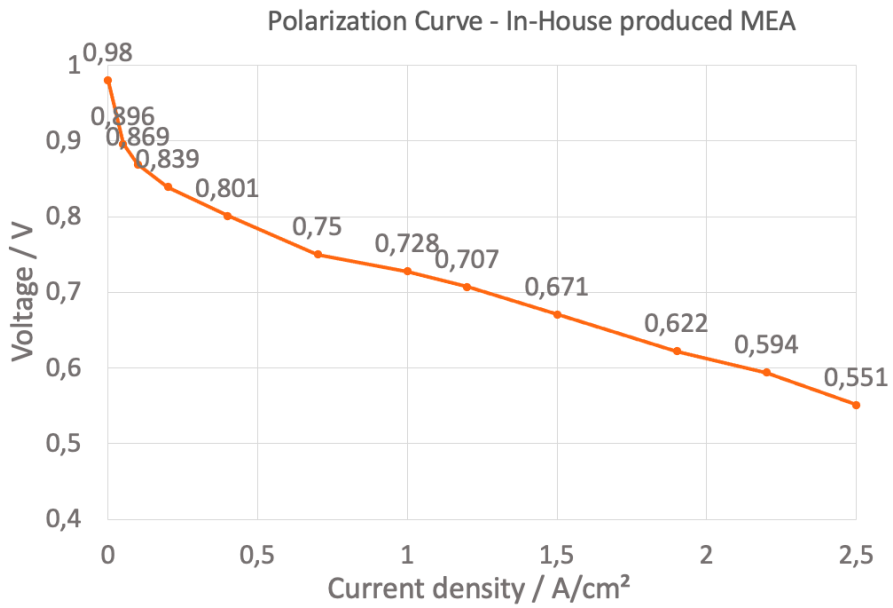


**Figure B.5:** Polarization curve for state of the art MEA produced in house, tested during normal operating conditions.

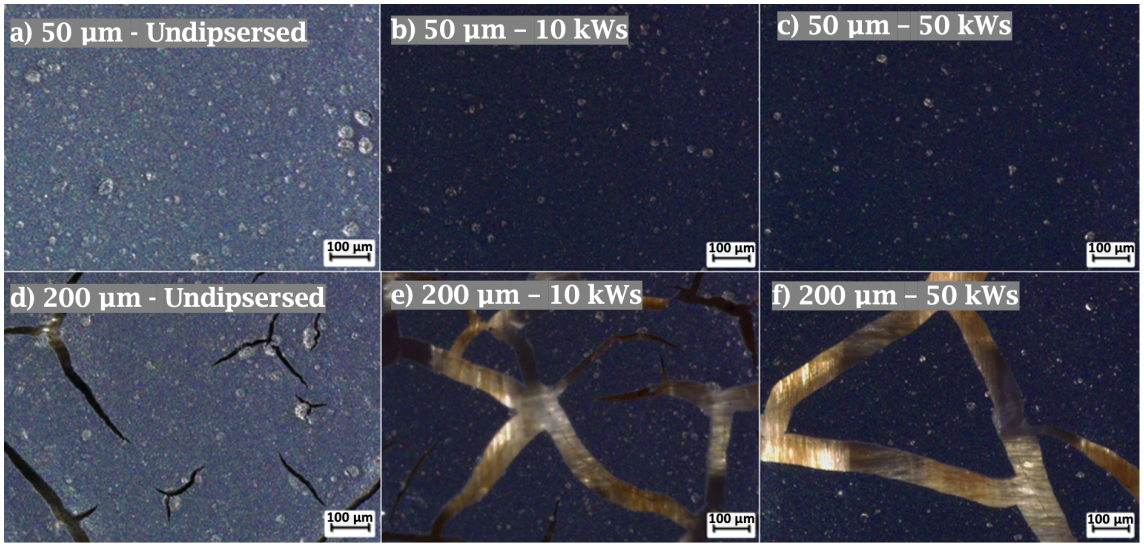


**Figure B.6:** Micrographs with 200x magnification of electrodes made with 50 $\mu$m and 200$\mu$m gap height from ink with KB 3000 catalyst and SSC ionomer left undispersed and dispersed to 10 and 50 kWs.

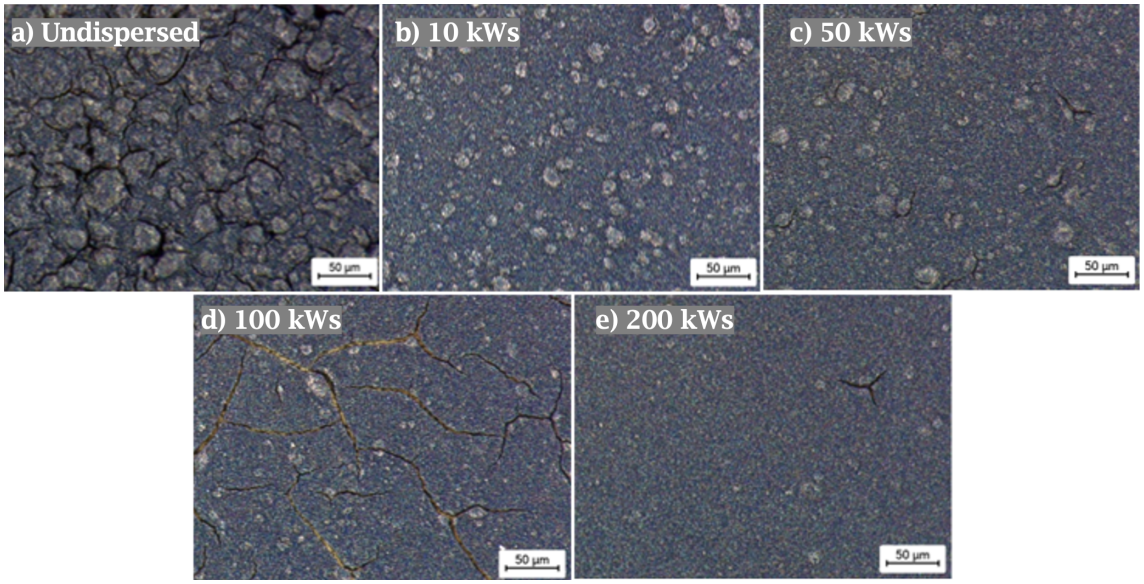


**Figure B.7:** Micrographs taken with 500x magnification of 200 $\mu$m thick coatings form the ink with GCE catalyst and SSC ionomer undispersed or dispersed to 10, 50, 100 or 200 kWs.

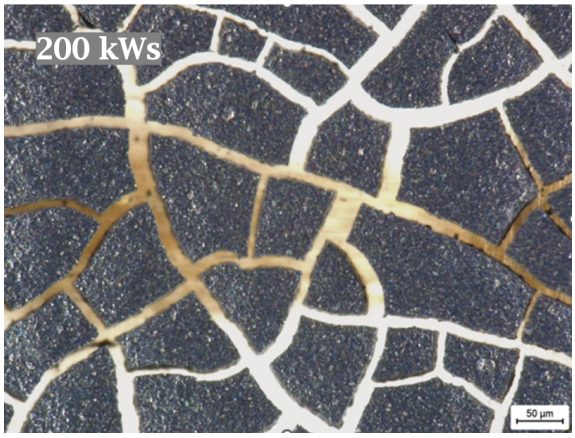


**Figure B.8:** Micrograph taken with 500x magnification of a coating with 200 $\mu$m gap height from the ink with HCE catalyst and SSC ionomer dipsersed to 200 kWs in the flow cell.

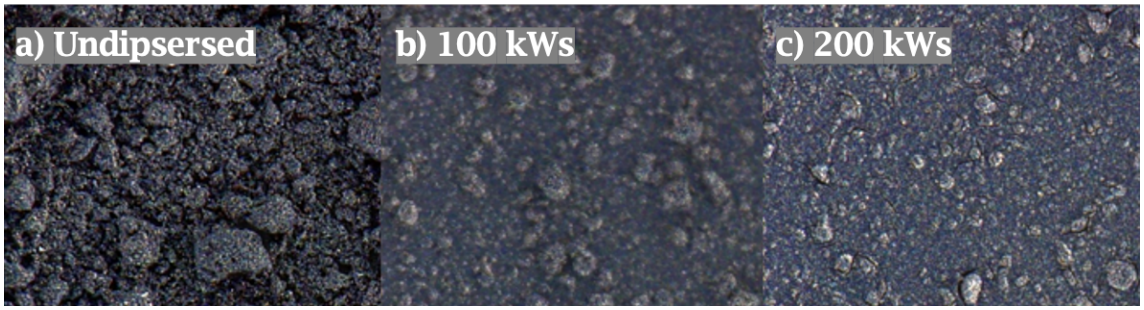


**Figure B.9:** Micrographs with 500x magnification of electrodes made with 50 $\mu$m gap height from ink with HCK catalyst and LSC ionomer left undispersed and dispersed to 100 and 200 kWs.

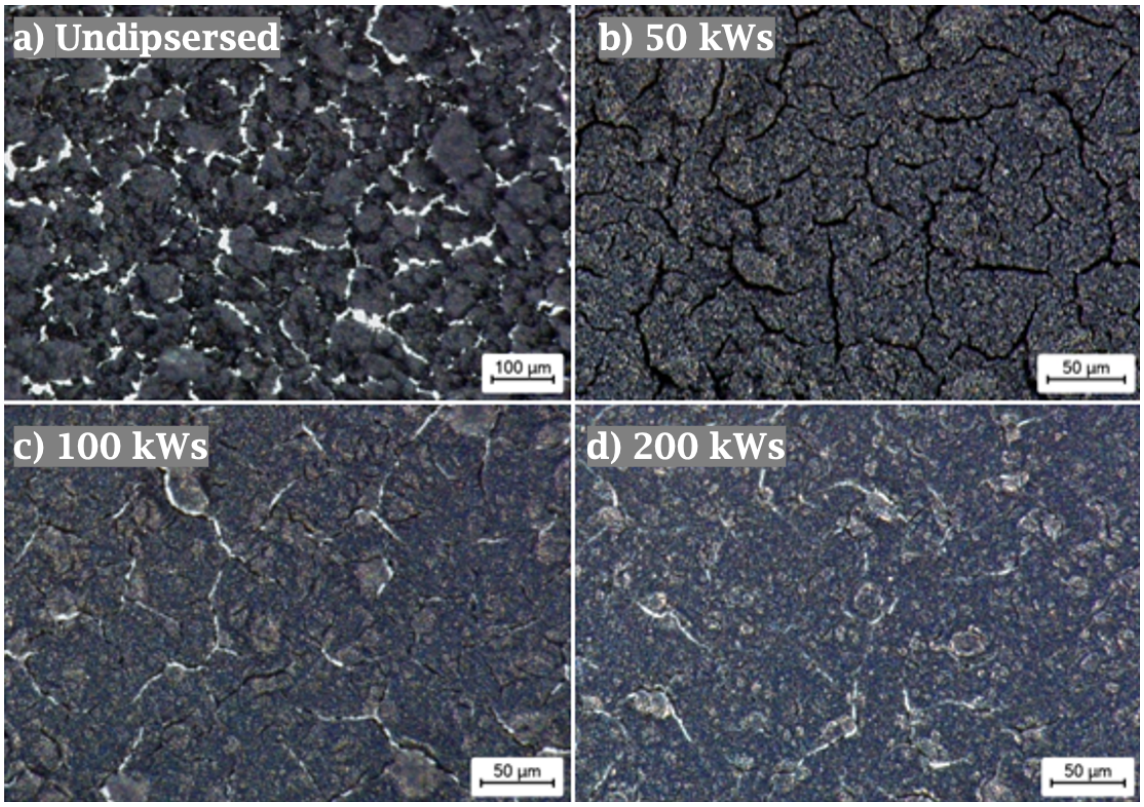


**Figure B.10:** Micrographs of electrodes made with 200 $\mu$m gap height from ink with HCK catalyst and LSC ionomer left undispersed and dispersed to 50, 100 and 200 kWs. Micrographs a is taken with 200x magnification and b,c and d with 500x magnification.

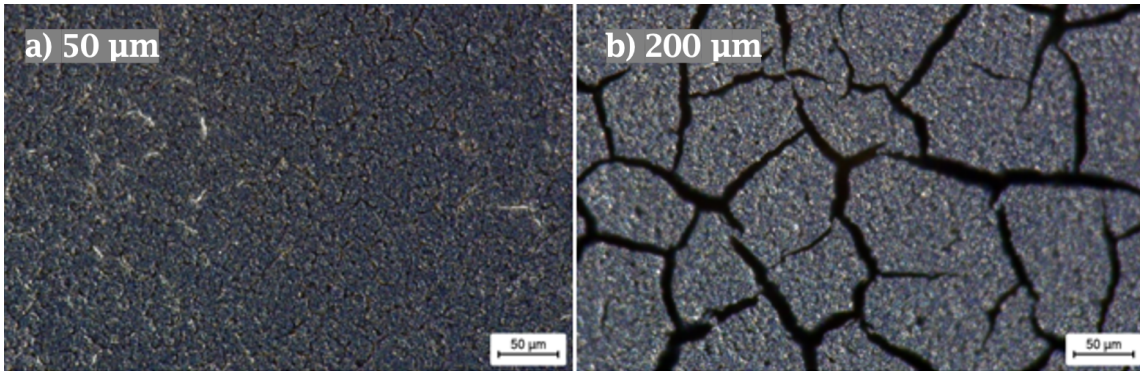


**Figure B.11:** Micrographs with 500x magnification of electrodes made with 50 and 200 $\mu$m gap height from ink with HCE catalyst and LSC ionomer dispersed to 200 kWs with the flow cell.

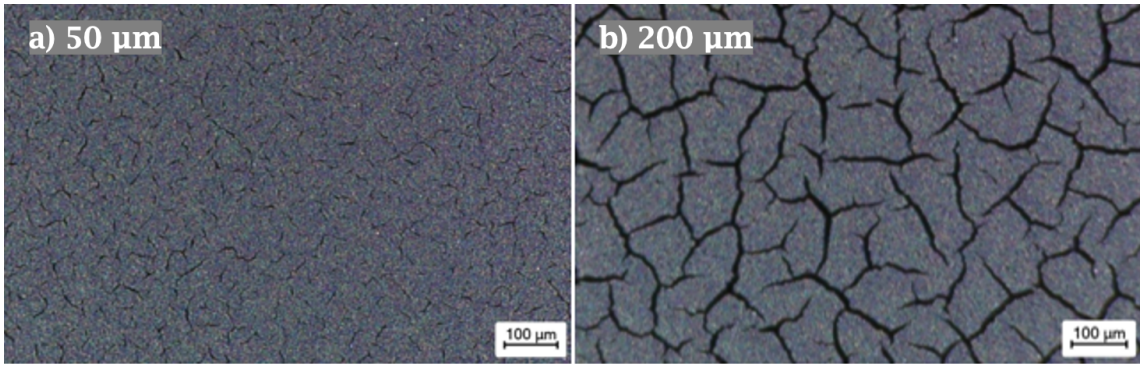


**Figure B.12:** Micrographs with 200x magnification of electrodes made with 50 and 200 $\mu$m gap height from ink with GCE catalyst and SSC ionomer dispersed by bead-milling for three days.

**DEPARTMENT OF PHYSICS**
**CHALMERS UNIVERSITY OF TECHNOLOGY**
Gothenburg, Sweden
www.chalmers.se


CHALMERS
UNIVERSITY OF TECHNOLOGY